March 2010

# Au NPs doped Photoresist Derived Carbon as a Substratum For Nerve Cell Culture

Chunwei Kuo
*Worcester Polytechnic Institute*

# Au NPs doped Photoresist Derived Carbon as a Substratum For Nerve Cell Culture

**A Major Qualifying Project Report**

**Submitted to the Faculty of the**

**WORCESTER POLYTECHNIC INSTITUTE**

In partial fulfillment of the requirements

for a Bachelor of Science Degree

in the field of Chemical Engineering

By:


_____

Chunwei Kuo


Approved by Project Advisor: Susan Hong Zhou

_____

Date: March 3rd, 2009

## Acknowledgements:

I would like to thank Professor Zhou for her guidance throughout the course of the project. Professor Bao at Umass Medical School also assisted with the cell culture protocols. I would also like to thank Dr. Jianlong Wang and Peter Hefti for their help on substrate fabrication and surface characterizations.

## Abstract

Gold nanoparticles (Au NPs) doped carbon film roughly of two micrometer thickness was prepared by pyrolysis of the mixture of photoresist and Au NPs on silicon wafers at a temperature of 1000$^{o}$C. Film loss assessment, cyclic voltammetry, atomic force microscopy and gionometer were used to evaluate the characters of the prepared film. The result indicated that the overall surface energy of the substrate increased with the increasing concentration of the doped Au NPs. The cyclic voltammetry results proved the pyrolyzed carbon film to have very similar electrochemical properties to the standard glassy carbon, which will provide a potential application for electrochemistry and controlled nerve cell culture. Based on these characters, the Au NPs doped carbon film was used as a substrate to accelerate the growth of nerve cell. Cell adhesion and morphology assays demonstrated that the attachment and differentiation on Au NPS doped carbon film is better than that on carbon, silicon and Poly-Lysine (PL) coated glass substrate due to its higher surface energy. Our AFM results also proved that surface energy is a more dominating factor than surface roughness in nerve cell-surface interactions. Importantly, the PC12 cells could be differentiated and grown on the Au NPs doped carbon even in the absence of nerve growth factor, which will benefit to understand the original growth of cell and reduce the cost of cell growth experiment.

# Table of Contents

Acknowledgements:.....- 2 -
Abstract.....- 3 -
List of Figures and Equations.....- 6 -
List of Tables.....- 8 -
1. Introduction:.....- 9 -
2. Background:.....- 11 -
2.1 Neuron Cells and Neurite Outgrowth.....- 11 -
2.1.1 Structure of Neurons:.....- 11 -
2.1.2 PC12 Cells:.....- 11 -
2.1.3 PC12 Cellular Response to Nerve Growth Factor.....- 11 -
2.2 Substrate Fabrication and Characterization:.....- 12 -
2.2.1 Glassy carbon fabrication – Spin Coating:.....- 12 -
2.2.2 Characterization of Photoresist-derived Carbon Film:.....- 13 -
2.2.3 Surface Energy Test:.....- 14 -
2.2.4 Atomic Force Microscopy.....- 15 -
2.3 Cell Culture.....- 16 -
2.3.1 Correlation between substrate topography and cell growth:.....- 16 -
2.3.2 The interaction between gold NPs and cells:.....- 17 -
2.3.3 Objective and Significance:.....- 18 -
3. Methodology:.....- 19 -
3.1 Synthesis of Au nanoparticles:.....- 19 -
3.2 Preparation of Au nanoparticle in organic solution:.....- 19 -
3.3 Spin Coating:.....- 19 -
3.4 Pyrolysis:.....- 20 -
3.5 Cell Adhesion Assay.....- 20 -
3.5.1 Cell Adhesion Test Method 1:.....- 20 -
3.5.2 Cell Adhesion Test Method 2:.....- 21 -
3.6 Cell Morphology Assay:.....- 21 -
3.7 Surface Energy Test:.....- 21 -
3.8 Atomic Force Microscopy:.....- 22 -
3.8.1 Taking the image:.....- 22 -

3.8.2 Analyzing the image: - 22 -
3.9 Film Loss Assessment: - 22 -
3.10 Cyclic Voltammetry: - 22 -
4. Results and Discussions: - 24 -
4.1 Pyrolysis: - 24 -
4.1.1 Method 1 Results: - 24 -
4.1.2 Method 2 Results: - 24 -
4.1.3 Method 3 Results: - 24 -
4.1.4 Method 4 Results: - 25 -
4.1.5 Method 5 Results: - 25 -
4.1.6 Method 6 Results: - 26 -
4.1.7 Method 7 Results: - 27 -
4.1.8 Method 8 Result: - 27 -
4.2 Cyclic Voltammetry Results: - 28 -
4.3 Film Loss Assessment - 29 -
4.4 Surface Energy Results: - 29 -
4.5 Cell Adhesion Assay - 31 -
4.5.1 Cell Adhesion Test Method 1: - 31 -
4.5.2 Cell Adhesion Test Method 2: - 32 -
4.6 Cell Morphology Assay: - 35 -
4.6.1 Cell Morphology Assay Trial #2: - 35 -
4.6.2 Cell Morphology Assay Trial #2: - 40 -
4.6.3 Cell Morphology Assay for gold samples of different concentrations: - 43 -
4.7 Atomic Force Microscopy - 44 -
5. Conclusion: - 46 -
Works Cited - 47 -
Appendix: - 50 -

# List of Figures and Equations

Figure 1: Factors Affecting Spin Coating ..... - 13 -

Figure 2: Basic principle of AFM. A sharp probing tip is mounted on a cantilever-type spring. The force between tip and sample causes cantilever deflections which are monitored by a deflection sensor. While scanning the samples a feedback-loop can keep the deflection constant (Meyer, Atomic Force Microscopy, Progress in Surface Science, Vol. 41, pp, 3-49, 1992) ..... - 16 -

Figure 3: Cracking and Peeling of the Carbon Film ..... - 24 -

Figure 4: Carbon/Iron (III) oxide Nanoparticle Film After Soaking in Water/ethanol ..... - 25 -

Figure 5: Carbon/gold nanoparticle Film After Soaking in Water/ethanol ..... - 25 -

Figure 6: Pyrolysis Method 5 Results ..... - 26 -

Figure 7: Pyrolysis Method 7 Results ..... - 27 -

Figure 8: CV Results for Pyrolysis Method 3(red) and 7(blue) ..... - 28 -

Figure 9: CV Result of Au Nanoparticle Films (blue) Compared to Carbon (red) ..... - 28 -

Figure 10: Contact Angle Comparisons ..... - 30 -

Figure 11: Surface Energy Comparison ..... - 31 -

Figure 12: Cell Adhesion Data for Different Substrates ..... - 32 -

Figure 13: Cell Adhesion Data for Different Substrates ..... - 32 -

Figure 14: Cell Adhesion Data for Different Substrates ..... - 33 -

Figure 15: Cell Recovery Rate of Different Substrates ..... - 33 -

Figure 16: Adhesion Data for Gold Nanoparticles of Different Concentrations ..... - 34 -

Figure 17: Cell Recovery Rates for Gold Nanoparticles of Different Concentrations ..... - 34 -

Figure 18: Differentiation of Cells on Carbon Surface without the Presence of NGF ..... - 35 -

Figure 19: Cells on PL Coated Glass Samples ..... - 36 -

Figure 20: Cells on Carbon with Gold Nanoparticles Surfaces ..... - 36 -

Figure 21: The Effect of NGF on Carbon Substrates ..... - 37 -

Figure 22: The Effect of NGF on Carbon+Au NPs Substrates ..... - 37 -

Figure 23: The Effect of NGF on PL Coated Glass ..... - 38 -

Figure 24: Neurite Length for Non-NGF Samples ..... - 39 -

Figure 25: Neurite Length for NGF Samples ..... - 39 -

Figure 26: Cell Body Area of Non-NGF Samples..... - 40 -

Figure 27: Cell Body Area of NGF Samples..... - 40 -

Figure 28: Neurite Length for Non-NGF Samples ..... - 41 -

Figure 29: Neurite Length for NGF Samples ..... - 41 -

Figure 30: Cell Body Area for Non-NGF Samples ..... - 42 -

Figure 31: Cell Body Area for NGF Samples ..... - 42 -

Figure 32: Neurite Length for Gold Samples of Different Concentrations ..... - 43 -

Figure 33: AFM Images of Bare Carbon (A1), 0.5ml Au (C1) and 3ml Au (D1)..... - 44 -

Figure 34: Schematic Relationship between Surface Roughness, Surface Energy, and Their Respective Influence on Cellular Adhesion Strength (Hallab et al.)..... - 45 -

Figure 35: The effect of NGF on the 0.5ml Au samples ..... - 54 -

Figure 36: The effect of NGF on the 1ml Au samples ..... - 54 -

Figure 37: Morphology of cells on the 3.0ml Au samples..... - 55 -

Figure 38: Effects of NGF on Glass+PL samples ..... - 55 -

Equation 1: Young's Equation..... -14-

Equation 2: Dupre Equation..... -14-

Equation 3: Young-Dupre Equation..... -14-

Equation 4: Surface Energy Formula (Robertson et al.)..... -14-

# List of Tables

Table 1: Pyrolysis Procedures ..... - 20 -

Table 2: Result from Method 6 of Pyrolysis ..... - 26 -

Table 3: Film Loss Assessment Results ..... - 29 -

Table 4: Cell Adhesion Trial 1 (Method 2) ..... - 50 -

Table 5: Cell Adhesion Trial 2 (Method 2) ..... - 50 -

Table 6: Adhesion on Gold NPs of different concentrations (Method 2) ..... - 51 -

Table 7: Cell Adhesion (Method 1) ..... - 51 -

Table 8: Surface Energy (Water) ..... - 52 -

Table 9: Surface Energy (Formamide) ..... - 53 -

# 1. Introduction:

The interactions between cells and substrates are important for the development of prosthetics and implantable devices. Biocompatibility is the key factor dictating those interactions. It has long been proven that glass slides that are used in nerve cell cultures are biocompatible and is the standard substrate when it comes to nerve cell culture. However, there are many more substrates that have not been investigated in the past and could potentially provide better substratum for nerve cell culture.

The first use of carbon as a biomaterial was in the late 1960s. It has become an industry standard currently mainly due to its advantageous properties. Carbon does not trigger adverse reactions when implanted in the human body hence making it more biocompatible than other substrates. Furthermore, it is thromboresistant making it an important agent to prevent blood clotting. It also provides good durability, wear resistance and strength. Therefore, carbon is used as the manufacturing material for prosthetic heart valves and orthopedic joints. Millions of implants made out of carbon have been implanted to date.

Due to many practical uses of carbon, a lot of microfabrication procedures of carbon structures have been investigated in the past. Current processing technology such as focused ion beam, and reactive ion etching are too costly and time consuming. Until recently, a more innovative way of carbon microfabrication methods were reported. These studies have fabricated glassy carbon using photolithography and pyrolysis. The heat treatment of 1000$^{o}$C enabled the conversion of polymeric microstructures to free-standing glassy carbon in an inert nitrogen environment. The electrochemical properties of the pyrolyzed carbon film have been widely studied. The result revealed that electrochemical reactions on pyrolyzed photoresist exhibit reaction kinetics comparable to those on glassy carbon [6,7]. This fabrication technique allows the patterning of the surface by lithography techniques which lead to the possibility of fabricating a wide variety of repeatable shapes.

However, these works are all focusing on the fabrication and application of bare pyrolyzed carbon film, the metal nanoparticles doped carbon film is never reported before. Nanotechnology has been a very widely investigated field of research in the recent years. The unique properties of nanoparticles make them ideal for many of the biomedical application. The three key areas that have been drastically improved due to the discovery of nanoparticles are cell separation, drug delivery and bioimaging. Studies have been done in the past showing that smaller nanoparticles (10-30nm) could be easily up-taken by human cells and larger nanoparticles could affect the overall cellular morphology due to its surface tension. Even though Au NPs were proven to be cytotoxic to cancer cells, the nerve cell viability is much higher with the presence of Au NPs.

Therefore, the specific aim of this project is to combine the advantage of photoresist-derived carbon with nanotechnology to fabricate the Au NPs doped photoresist-derived carbon and investigate their application in accelerating cell growth and locating cell differentiation of PC12 cells. This substrate takes advantage of the unique properties of nanoparticles and abilities to pattern the carbon substrates. The roughness gradient created by doping the Au NPs allows us to investigate the correlation between surface roughness and cellular response. In addition, surface energy could also be changed by doping

different concentrations of Au NPs and this enables us to observe the effect that surface energy has on the cellular adhesion and morphology.

# 2. Background:

## 2.1 Neuron Cells and Neurite Outgrowth

### 2.1.1 Structure of Neurons:

Axons and dendrites are the two structurally and functionally distinct parts of neurons. These two parts allow neurons to receive, process, and transmit information. In most cases, neurons are comprised of one axon and multiple dendrites. The composition of proteins and organelles in axons and dendrites are different as well. Axons are long and thin and they have a uniform caliber at all distances from the cell body. In addition, axons also branch at right angles. Dendrites, on the other hand, are shorter and thicker when compared to axons. The dendrite caliber decreases as they get further away from the cell body. Unlike the axons, the dendrites branch in Y shape. Generally, neurons initially generate several equivalent neurites, and that neurons begin to polarize when one neurite becomes an axon; the other neurites then become dendrites. From the previous studies, it takes 24 hours after planting in order for the axon to be formed. The neurites normally had to reach a length of 20um for the formation of axon to occur. Once the axon is formed, the neurons undergo a transition between the unpolarized and polarized state. The polarity of the neuron could be modified by cutting the axon because one of the other neurites will then become the new axon.

### 2.1.2 PC12 Cells:

The cell line used for this project was PC12. It is a cell line derived from a pheochromocytoma of the rat adrenal medulla. PC12 cell line was chosen because of its ability to differentiate once the Nerve Growth Factor has been applied. PC12 cells stop proliferating once NGF has been applied. Several investigations have been done on the differentiation of PC12 cells. Differentiation could be induced by various factors such as cytokines, nerve growth factor (NGF), basic fibroblast factor and epidermal growth factor (EGF). By counting the number of cells extending neurites of lengths more than twice the cell diameter, the neurite outgrowth of PC12 cells could be assessed. However, taking images and measurements are too time-consuming when running a large batch of samples. Therefore, examining the expression of neuronal markers or metabolic enzyme activity are the alternative means of assessing neurite outgrowth. In the study done by Ohuchi et al., 6 different agents were used to induce neurite growth and NGF has shown to have the best result.

### 2.1.3 PC12 Cellular Response to Nerve Growth Factor

Several methods to both understand and enhance axonal re-generation have been investigated recently. It was well established that PC12 respond very well to the application of NGF. Kapur et al. tried to develop an appropriate method to create stable, immobilized concentration gradient of growth factors in p(HEMA) gels. NGF was chosen to apply to PC12 cells because it has been well characterized. Kapur et al have proved that as the concentration of NGF increases, the length of the resulting neurite is longer. Concentration of NGF and neurite length has a directly proportional relationship. PC12 cell neurites were observed to be thicker when cultured on immobilized NGF than when cultured in the

presence of soluble NGF. However, with the immobilized NGF gradient, the direction of the neurites could be altered.

## 2.2 Substrate Fabrication and Characterization:

There are a lot of forms of carbon in nature. Forms like diamonds, graphite, coke and glassy carbon are all made out of carbon. Focused ion beam and reactive ion etching were the two carbon processing technologies, however, they are very time consuming and expensive. In addition, the low feature resolution, poor repeatability of carbon composition as well as the widely varying properties of the resulting device limit the application of screen printing of commercial carbon inks for microfabricated carbon structures. Therefore, glassy carbon has received an enormous amount of attention due to its wide range of electrochemical stability, excellent biocompatibility, low cost and ease of fabrication.

### 2.2.1 Glassy carbon fabrication – Spin Coating:

Silicon or silicon dioxide wafers are the most common substrates that are used for the fabrication of glassy carbon films. Wafers are normally cleaned first in acetone bath and then sonication in methanol or ethanol to remove the dirt or impurities off the wafer surface. Singh et al. cleaned the wafer using acetone and isopropyl to remove any traces of dirt, grease and dust on the surface. Wafers were then put into the oven to dry to remove any of the unnecessary mixture. The spin coating speed ranged between 3000-6000 rpm for 30s. Spin coating has been a vital process for the application of thin film onto the surface. The photoresist or any other liquid are normally deposited on the center of the wafer and the centripetal acceleration will cause the resin to spread to and eventually off the edge of the substrate leaving a thin film of photoresist on the surface. The degree of centrifugal force applied to the liquid and the velocity and characteristic turbulence of the air immediately above it are all affected by the speed of the substrate. The spin speed is the key determinant to the final film thickness. Film thickness is largely a balance between the forces applied to shear the fluid toward the edge of the substrate and the drying rate which affects the viscosity of the liquid. In the case of photoresist, it is a highly viscous liquid therefore a very fast spin speed is required to evenly spread the photoresist across the silicon wafer before it dries out. Figure 1 explains the relationship between film thickness, spin speed and spin time. Clearly, as spin speed increases, the film thickness decreases exponentially. As the spin time increases, the film thickness decreases.

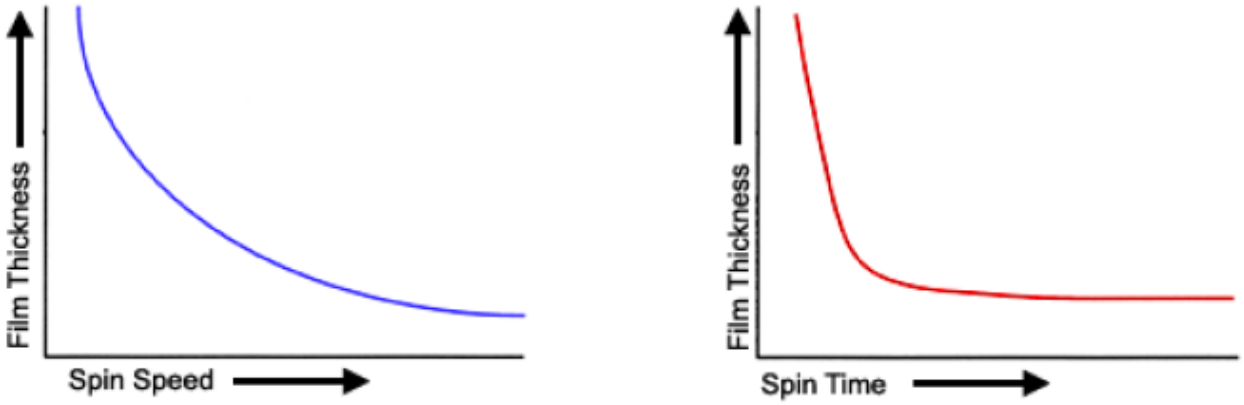


**Figure 1: Factors Affecting Spin Coating**

### 2.2.2 Characterization of Photoresist-derived Carbon Film:

Mechanistic study of redox systems could be done in many ways, however, cyclic voltammetry (CV) is perhaps the most effective and versatile electroanalytical techniques available. The electrode potential is scanned rapidly in search of the redox couples. The couple can be characterized from the potentials of peaks on the cyclic voltammogram and from the change caused by variation of the scan rate. CV is normally the first test performed in the whole electrochemical analysis procedure.

Kim et al. did studies on pyrolyzed photoresist films. They focused mainly on the surface characterization of the fabricated carbon film. SEM, TEM, Thermal Gravimetric Analysis and Four Point Probe were used for characterization. It was well documented that carbon films fabricated over 700$^{o}$C showed similar electrochemical behavior to glassy carbon. The study also showed that carbon film fabricated at higher temperature tend to have lower resistance. For a positive photoresist like AZ4330, at 1000$^{o}$C, the resistance is at about 50 ohms/square. Cyclic voltammetry was done to further prove that the pyrolyzed film does indeed behave like glassy carbon electrochemically.

Ranganathan et al. did a much more in depth electrochemical study in 2000 related to pyrolyzed photoresist film. The resistance test showed a good agreement with what was performed by Kim et al. In addition, they also did a film shrinkage measurement for carbon films that were pyrolyzed under different temperature range. At 1000$^{o}$C under nitrogen surroundings, it was reported that 80.51% of film loss is expected after pyrolysis. They also investigated on the resistivity of glassy carbon. The reported resistivity for GC was 4 micro ohms centimeter and the photoresist derived carbon at 1000C also showed the same value.

Teixidor et al. also employed a similar fabrication method of GC. However, they modified the surface by oxygen-plasma treatment in order to make the surface rougher.

### 2.2.3 Surface Energy Test:

One of the oldest equations that were used to calculate for surface energy was Young's equation. It is used to describe the balance of energies controlling the contact angle of the liquid drop on such a surface (equation 1). As shown in equation 2, Dupre proposed the idea of the thermodynamic work of adhesion, which is the reversible work done is separation of unit area of solid/liquid interface. Then the Young-Dupre equation was formed as shown in equation 3.

$$\gamma_s = \gamma_{SL} + \gamma_L cos\theta$$

**Equation 1: Young's Equation**

$$W_{ad} = \gamma_S + \gamma_L - \gamma_{SL}$$

**Equation 2: Dupre Equation**

$$W_{ad} = \gamma_L(1 + cos\theta)$$

**Equation 3: Young-Dupre Equation**

Dispersion (gamma d), polar (gamma p) and hydrogen bond (gamma h) are the three different intermolecular forces that contribute to the calculation of total surface energy. Normally, the polar and hydrogen bond forces are encompassed in a single term (gamma p). Therefore, in order to derive the total surface energy, 3 liquids are needed and the sum of the three different intermolecular forces will allow us to derive the total surface energy of the substrate.

Kennedy et al. measured the surface energy using Pearson correlation coefficient. They converted the water contact angle into surface energy by the equation shown in equation 4 where "x" was denoted to water contact angle.

$$\text{S.E.} = 74.5 - 0.372x - 0.00181x^2$$

**Equation 4: Surface Energy Formula (Robertson et al.)**

Hallab et al did an investigation on cellular response to substrates of different surface energy. They derived their total surface energy and the dispersive and polar components of surface energy from contact angle measurements using six liquids on each material: PBS, glycerin, 30W-oil, DMEM, dimethylsulfoxide (DMSO), and benzene. They applied 2*ul*/drop of liquid on to the substrate and the contact angle was measured using a digital camera connected to the eyepiece of an inspection zoom microscope. They followed the Young-Dupre equation to determine the components of polar (acid/base) and dispersion surface tensions of material surface A and liquid B. Schakenraad et al. have also done the same thing to retrieve for surface energy.

### 2.2.4 Atomic Force Microscopy

The predecessor of the atomic force microscopy is the scanning tunneling microscopy (STM). Back in the day, STM was a useful tool in surface science because of its ability to characterize surfaces of metals and semiconductors in real space on an atomic scale. One of the major drawbacks of STM is the requirement of sample conductivity. Therefore, in 1986, Binning et al proposed a new type of microscope that could overcome this drawback. The STM measures the surface properties by measuring tunneling currents between a probing tip and sample, AFM on the other hand, measures the forces on the atomic scale. AFM is a synthesis of the mechanical profilometer, using mechanical springs to sense forces and the STM, using piezoelectric transducers for scanning. A lot of the other scanning microscopes were invested based on the basic principles of the AFM to measure forces or to measure interactions between sharp probing tip and sample surface.

There are several fundamental and basic principles of force microscopy. The probing tip is attached to a cantilever-type spring. The cantilever is deflected in response to the forces between tip and sample. By scanning the sample relative to the probing tip and digitizing the deflection of the lever or the z-movement of the piezo as a function of the lateral positions x,y, the images could be taken. Since the forces between the probing tip and the samples are very small, non-destructive imaging is possible. There for two force regimes that could be distinguished in the AFM, the contact and the non-contact mode. Under non-contact mode, the tip-sample separation ranges between 10 to 100nm. Forces such as van der walls, electrostatic, magnetic or capillary forces can be sensed and give information about surface topography, distribution of charges, magnetic domain wall structure or liquid film distribution. Under the contact mode, the ionic repulsion forces allow the surface topography to be traced with high resolution since the sample is in contact with the tip. Furthermore, under appropriate conditions, frictional forces and elastic or plastic deformations can be detected under appropriate conditions.

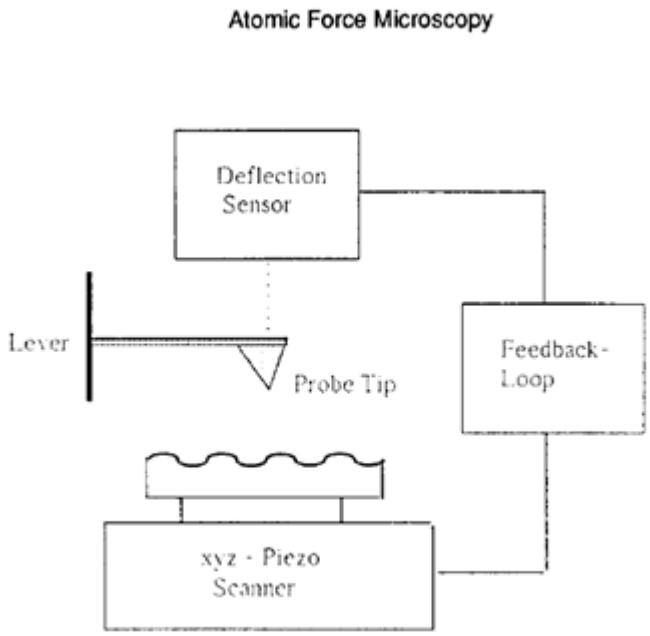


**Figure 2: Basic principle of AFM. A sharp probing tip is mounted on a cantilever-type spring. The force between tip and sample causes cantilever deflections which are monitored by a deflection sensor. While scanning the samples a feedback-loop can keep the deflection constant (Meyer, Atomic Force Microscopy, Progress in Surface Science, Vol. 41, pp, 3-49, 1992)**

## 2.3 Cell Culture

### 2.3.1 Correlation between substrate topography and cell growth:

There are many different physical properties of the substrate that could affect the adhesion of cells to the surface. Roughness is one of the most influential. Fan et al. did an investigation in adhesion of neural cells on silicon wafer with nano-topographic surface. The roughness of silicon wafer was controlled by setting up different etching time periods (HF solution was used to etch the silicon surface. SEM was employed to look at the cell adherence and viability. They proved that cells (nigra cells) could adhere better and survive much better on the HF treated surface than on the control surface. The AFM images also have shown that the HF treated wafers are much rougher than the control. From this experiment, they came up with a qualitative theory that rough surface promotes cell adhesion, however, there has yet to be a quantitative theory that could be used to explain this phenomena.

Another roughness-cell correlation was done by Huang et al. in 2004. Surface roughness ranging from 0.05um to 1.2um was tested. The aim for their experiment was to find out the optimal range of roughness that leads to the highest adhesion rate. It showed that a surface roughness at 0.15um had the optimal cell adhesion behavior. A mathematical relationship between cell adhesion and surface roughness could not be determined. There seemed to be an optimal range of roughness for the cells to adhere the most as report by Huang et al.

The substrate topography and chemistry affect not just the cell adhesion, but also orientation, proliferation and growth. Ponsonnet et al. did an experiment investigating those relationships in 2002. Teixidor et al. cultured NSC-34 cells on carbon on silicon dioxide wafer, carbon on quartz, ITO on glass and oxygen plasma treated carbon. Each of the substrates has varying roughness. An interesting observation was made that the NSC-34 cells prefer to adhere to the carbon covered area but with little spreading and round shape. When the cells were put onto the plasma treated carbon, differential attachment took place which means that the rougher surface could also lead to not just cell adhesion but also cell differentiation. Theoretically, cell adhesion should increase with increasing surface energy and decreasing hydrophobicity. However, cell proliferation and migration also depends on the cell-surface interaction. The interfacial force is the governing factor of cell adhesion and cell spreading. Studies have been done that the neurons have a preferred optimal range of roughness that will provide the greatest interfacial force leading to higher cell adhesion and spreading. They have also observed that carbon on silicon dioxide performed very well in cell adhesion when compared to carbon on quartz and ITO on glass.

### 2.3.2 The interaction between gold NPs and cells:

As the recent nanotechnology advances, the small sized nanoparticles are used for many of the biomedical applications. Most importantly, gold NPs are known to have the potential to do cancer detections. Patra et al. did an experiment investing the cell-specific response to gold NPs (GNP) in 2006. Carcinoma lung cell line A549, BHK21 (Baby Hamster Kidney) and HepG2 (Human hepatocellular liver carcinoma) were tested during the experiment. It was found that the GNPs actually caused A549 cell death. However, BHK21 and HepG2 remained unaffected by the GNPs. The A549 cells were exposed to GNPs for 48 hours which changed the cellular morphology. The A549 cells became more circular because of the physical stress implied by the presence of the GNPs. On the other hand, there was no change in cellular morphology for the other 2 cells lines. Under the florescence microscope, a significant change in nuclear morphology was observed in the A549 cell lines. It was also reported that the accumulation of GNPs is localized in specific cellular domains. This conclusion was derived by using the fluorescence microscope and confocal microscopic technique. It was concluded by Patra et al. that the GNPs nanosurface evokes a cell-specific death response. However, the GNPs clearly did not affect the BHK21 cells and the HepG2 cells in terms of viability and cellular morphology.

In 2007, Wei et al. did an investigation on the disruption of HepG2 cell adhesion by gold nanoparticles and paclitaxel disclosed by in situ QCM measurement. Even though the experiment was meant to disrupt tumor cell adhesion, it is important to note that the cytotoxicity of GNPs was being tested also in this literature. Methylthiazol Tetrazolium (MTT) essay was used to test for the cytotoxicity of the GNP. With just the GNP, 95% of the cells survived after 8 hours of incubation and 80% survived after 24 hours of incubation. Comparing it with paclitaxel and the mixture of GNPs and Paclitaxel, the GNPs provided doubled or even tripled cell viability which could be further concluded that GNPs are not cytotoxic to cells. The other important point which they proved is that the GNPs could interrupt cell adhesion. QCM was used to test for the cell adhesion and when GNPs were present, the frequency raised meaning that the cells were being detached from the surface by the GNPs.

Mao et al. did a thorough investigation on the interaction of the GNPs to cells. It was found that after 48 hours of incubation, the GNPs with an average diameter of 100nm were uptaken by the cells and could be found in the compartments resembling endosomes and cytoplasm, and on the nuclear envelop and even inside the nucleus. It was also reported that 0.05mg/ml concentration of GNPs did not affect the cell viability even after 4 days of incubation. When the cells were co cultured with bare GNPs, the cytoskeleton of the cells was changed to a more rounded shaped when compared to the control. This investigation coated the GNPs with Poly-Caprolactone (PCL). The purpose of PCL was to reduce GNP cytotoxicity and their result had proved that even at 1mg/ml of GNP+PCL concentration, the cells remained relatively viable when compared to bare gold nanoparticles

### 2.3.3 Objective and Significance:

From the literature reviews, the standard for nerve cell culture is to use poly-lysine (PL) coated glass. Even though PL coated glass enhances the cell adhesion to the glass substrate, the adhesion rate could be improved by developing more biocompatible substrates such as photoresist-derived carbon. Photoresist-derived carbon offers the capabilities to pattern the roughness and surface energy of the substrate by doping nanoparticles at various concentrations. The objective of this project is to investigate the relationship between nerve cell behavior and physical properties such as roughness and surface energy of the carbon substrate. This experiment will allow us to understand the biocompatibility of gold nanoparticles doped carbon compared to PL coated glass. Furthermore, the understanding from this project will help in the development of primary neuron culture and stem cell engineering. Prosthetic implant devices could also use nanoparticle doped carbon as the raw material if nanoparticle doped carbon give a higher rate of cellular adhesion and degree of cellular differentiation.

# 3. Methodology:

## 3.1 Synthesis of Au nanoparticles:

100 mL of 1mM $HAuCl_4$ (4 mL 1% (w/w) $HAuCl_4$ solution dissolved in 96 mL $H_2O$) was brought to a reflux while stirring and then 10 mL of a 38.8 mM trisodium citrate (10 mL 1.14% (w/w) trisodium citrate) solution was added quickly, which resulted in a color change of the solution from pale yellow to deep red. After the color change, the solution was refluxed for an additional 15 min and left to cool to room temperature.

## 3.2 Preparation of Au nanoparticle in organic solution:

Stock solution of gold nanoparticle in water was previously prepared. In order for the gold nanoparticles to successfully mix with photoresist, an organic solvent (i.e. toluene) was needed instead of water. 10 mM of undecanoic acid (uDA) was prepared in solution with 50 ml of ethanol and 0.11 grams of undecanoic acid in powder form. Solution was prepared in a 50 ml volumetric flask. 150 micro-liter of the uDA solution was pipetted into a 15 ml of gold nanoparticle stock solution. The uDA/gold nanoparticle was stirred using the magnetic stirrer for 30 minutes and left in room temperature overnight for the reaction to go to completion. 10 mM of CTAB was prepared in solution with 100 ml of deionized water and 0.36445 grams of CTAB in powder form. Solution was prepared in a 100 ml volumetric flask. The solution was sonicated to enhance better mixing. 150 micro-liter of the CTAB solution was pipetted into the previously made uDA/gold nanoparticle mixture. The final uDA/Gold nanoparticle/CTAB solution was stirred using a magnetic stirrer for 30 minutes. The final solution was left under room temperature for 30 minutes for the reaction to go to completion.

5 ml of toluene is then added to the uDA/Gold nanoparticle/CTAB solution and stirred on a magnetic stirrer for 5 minutes to enhance better transfer of nanoparticles from water to toluene.

## 3.3 Spin Coating:

The wafers are first sprayed using nitrogen gas to clean the dust on the surface. Then the wafer is put into a large petri dish filled with acetone. The dish is agitated in order to remove any of the impurities from the silicon wafer surface. After 4 minutes of acetone bath, the wafer is sonicated in ethanol for another 4 minutes. Wafer is then put into another large petri dish with running deionized water for 4 minutes. The wafer is sprayed by nitrogen gas and then put onto the spin coater using 3000 rpm for 10 seconds to make sure there are no water droplets on the wafer. The wafer is then soft-baked at 110C in an oven for 2 minutes to make sure it is completely dried. Wafer is left to cool for 2 minutes and then is ready to be spin coated.

3ml of the previously made Au nanoparticle solution is mixed with about 8ml of photoresist in a separate vial. 0.1ml of the previously made $Fe_3O_4$ nanoparticle solution is mixed with about 8ml of photoresist in another vial.

First, the wafer is put onto the center of the vacuum of the spin coater. Spin coater is turn on and spun at 3000 rpm for 5 seconds to make sure the wafer is placed in the correct manner. Then, about 2ml of S1813 photoresist or photoresist/nanoparticle solution is added onto the wafer and the wafer is spun at

3000 rpm for 90 seconds. The coated wafer is soft-baked at 110C in the oven for 2 minutes. The coated wafer is then taken out of the oven and left to cool for 2 minutes. The coated wafer is then ready for another spin coat or pyrolysis. Each wafer is spin coated 4 times and with about 2ml of photoresist each time to make sure there will be the same thickness of carbon film after the pyrolysis.

## 3.4 Pyrolysis:

The wafers are cut into 22mm X 22mm square chips using a maker and a ruler. The chips are loaded on to boats (bare silicon wafers). The boats are them put into a large tube. The tube is put into the furnance and sealed with a nitrogen gas source. The nitrogen gas tank is turned on allowing nitrogen gas to flow through. Inert nitrogen gas environment is created by allowing the gas to flow at 100ccm for 10 minutes. The furnace is turned on and the heat rate is adjusted to 2°C/min. When the temperature reached 300°C, the heat rate is adjusted to 10°C/min. This is one of the working procedures, other procedures may be found in the following table.

**Table 1: Pyrolysis Procedures**

| Method | Photoresist | Temperature Range | Heat Rate | Temperature Range | Heat Rate |
|---|---|---|---|---|---|
| 1 (05/26/2009) | S1822 | 22°C-300°C | 2°C/min | 300°C-1000°C | 10°C/min |
| 2 (06/05/2009) | S1813 | 21°C-300°C | 2°C/min | 300°C-1000°C | 8°C/min |
| 3 (06/08/2009) | S1813 | 21°C-300°C | 2°C/min | 300°C-1000°C | 8°C/min |
| 4 (06/10/2009) | S1813 | 21°C-430°C | 2°C/min | 430°C-1000°C | 10°C/min |
| 5 (06/23/2009) | S1813 | 22°C-340°C | 2°C/min | 340°C-1000°C | 8°C/min |
| 6 (06/24/2009) | S1813 | 21°C-300°C | 2°C/min | 300°C-1000°C | 8°C/min |
| 7 (06/22/2009) | S1813 | 22°C-300°C | 2°C/min | 300°C-1000°C | 9°C/min |
| 8 (06/29/2009) | S1813 | 22°C-310°C | 2°C/min | 310°C-1000°C | 10°C/min |

## 3.5 Cell Adhesion Assay

### 3.5.1 Cell Adhesion Test Method 1:

Samples were separated into 11 small petri dishes. Samples were left to the exposure of UV light for 2 hours and left over night in the lab for sterilization purposes. On the next day, 6 samples were soaked in poly-lysine (PL) for 4 hours. The concentration for PL is 50ug/ml. After the samples are coated with PL, all the samples are washed with 1X PBS for 3 times. Cells were seeded 2.5 X $10^5$ cells/ml. There were 3ml of growth media with cells in each of the petri dishes. Samples are left in a 37°C oven overnight for the cells to adhere to the substrates. On the following day, NGF is applied to 6 of the samples. The concentration for NGF was 1:1000 v/v. Therefore 18 ul of NGF is mixed with 18ml of growth media in a 50ml vial. The vial is vortexed to enhance better mixing. The media of all the samples are changed, with or without NGF. Cells are allowed to adhere to the surface of the substrate for 2 days, and then the samples are ready for the cell adhesion test. First, the media is removed from all the samples. Samples are washed with PBS once and 0.5ml of trypsin is added to each of the samples. Samples are left to sit for 15 minutes under room temperature for the cells to be detached from the surface. 0.5ml of growth

media is added to each of the samples. Each sample is well pippetted to ensure there are no cell clusters and all the cells are detached from the surface. Cell numbers in each plate is counted using a microscope.

### 3.5.2 Cell Adhesion Test Method 2:

Samples were separated into 15 small petri dishes. Samples were left to the exposure of UV light for 2 hours for sterilization purposes. All the samples were washes with 1X PBS for 3 times right after UV light exposure. Cells were seeded at 1.32 X $10^5$ cells/ml. There were 3 ml of growth media with cells in each of the petri dishes. Samples are left in a 37°C oven overnight for the cells to adhere to the substrates. On the following day, NGF is applied to 4 of the samples. The concentration of NGF was 1:1000 v/v. Therefore, 12ul of NGF is mixed with 12ml of growth media in a 50ml vial. The vial is vortexed to enhance better mixing. The media for 4 other non-NGF samples is changed and the samples are put back into the incubator along with the 4 NGF samples. The remaining 7 non-NGF samples are ready for the cell adhesion test. The media of the 7 samples are removed and each sample is washed with 1X PBS once. 0.3 ml of trypsin is applied to each of the 7 samples and left under room temperature for 10 minutes. 0.7 ml of growth media is then added to each sample to complete the trypsinization process. Each sample is pipetted to reduce clusters of cells and to make sure all the cells are off the surface of the substrates. Cell number in each plate is counted using a microscope.

## 3.6 Cell Morphology Assay:

The remaining 8 samples from cell adhesion test method 2 are used for the cell morphology assay. The media of the samples are removed and 4% paraformaldehyde solution is applied for the purpose of fixing the cells on each substrate. Enough of paraformaldehyde is added to cover the substrate and the samples are left under room temperature for 5 minutes. The paraformaldehyde is removed and each substrate is washed 3 times with PBS. The previously prepared DiI solution is diluted with 100% ethanol in 1:1000 v/v ratios. 2 aliquots of 1ml DiI solution are made for staining purposes. DiI is applied to the substrate 20ul at a time for 1 minute. DiI is added continuously to prevent the cells from drying due to evaporation. Substrates are then rinsed with PBS once. Samples are taken out from the petri dish using tweezers and put on to glass. 20ul of mounting media is applied on top of the substrate and the cover slip is put to correctly mount the samples.

## 3.7 Surface Energy Test:

All the substrates were soaked in DI water over night to ensure the surface is cleaned and the carbon film was well attached to the silicon surface. Water, formamide and hexadecane were used fpr the surface energy test. The substrate was first loaded onto the Goniometer. The tip of the Goniometer was rinsed three times using DI water. 50ul of air was input into the tip to create a separation. 30ul of water, formamide or hexadecane was input into the tip. Each drop of liquid is 2ul and was placed onto the substrate by adjusting the height of the tip. Contact angle was then measured using the program "DropIMAGE". 5 droplet were put onto each slide and 3 slides were used for each substrate. A total of 15 contact angle measurement was made per substrate. Young's equation $S = \gamma_{LG}(\cos(\theta) + 1)$ was used to calculate for surface energy.

## 3.8 Atomic Force Microscopy:

### 3.8.1 Taking the image:

First the mounter was put onto a holder. The cantilever was loaded on to the mounter by using a tweezer. The cantilever used was produced by Veeco with a model number of TESP. The cantilever should be placed onto the mounter with care because it is very fragile. Once the cantilever was successfully loaded onto the mounter, the mounter was then mounted onto the AFM. The AFM was calibrated so that the cantilever was visible under the red light for scanning purposes. Once the tip of the cantilever was found, the bright red spot appeared on the computer screen, the red dot was adjusted so it was at the center of the graph. The illumination was set to 100 in order to adjust the cross inside the cantilever. One the preliminary set up was done; the substrate was loaded onto the AFM. "Amplitude Setpoint" and "Drive Amplitude" were adjusted to find the peak under the scope control button. Once the peak was found, the green mark was placed to the left of the peak. After finishing the calibration of the microscope, the illumination is set to 100. The position and zoom of the microscope is adjusted until a better view of the substrate is obtained. The microscope is then engaged by hitting the green button on the screen. Once the microscope is successfully engaged, scope trace is used to adjust the pattern of the yellow and white line. The two lines are adjusted to have similar patterns. Once the pattern is found, the substrate is traced from top to bottom. Image is captured during the trace. The microscope is disengaged after the trace is completed.

### 3.8.2 Analyzing the image:

The image is analyzed on the same computer connected to the AFM. The image is first loaded and then flatten in order to take the measurement. The image on the right side of the screen is used for the roughness measurement. The image is then analyzed through the program to determine the roughness. The RMS value is recorded as the roughness of the substrate.

## 3.9 Film Loss Assessment:

Film thickness and mass loss during fabrication are also quantified to provide better understanding of the film. By scraping a small area of the carbon film off with a razor blade, it is possible to measure the distance between the top of the remaining film and the wafer surface. Viewing the wafer through a Nikon microscope using a white light source and a 10X Mirou type double beam CF Plan EPI DI objective on a Physik Instrumente E-500.00 piezoelectric controller and measuring device, the wafer is aligned at a slight tilt so that it is not perpendicular to the microscope. The tilt of the sample makes phase contrast lines appear and distances may be measured by observing differences in focal length as reported by the piezoelectric controller while focusing on the stop of the film or the bare wafer.

## 3.10 Cyclic Voltammetry:

Au NPs doped carbon films were characterized by cyclic voltammetry (CV) to confirm the stability of the prepared Au NPs doped carbon films. The rectangular Au NPs doped carbon film was cleaned by sonification in water, anhydrous ethanol, and water again for five minutes each in a B25500A-MTH Ultrasonics Cleaner (VWR North America). The CV of Au NPs doped carbon film was recorded by

scanning from 0.0 to +0.60 V four times at a rate of 100mV/s in a 0.005 M $K_4[Fe(CN)_6]$ / $K_3[Fe(CN)_6]$ solution of PBS with Ag/AgCl as the reference electrode. A polished glassy carbon electrode is used as a standard and the electrochemical properties of Au NPs doped carbon films are compared with the glassy carbon electrode.

# 4. Results and Discussions:

## 4.1 Pyrolysis:

### 4.1.1 Method 1 Results:

As may be seen from figure 3, lots of cracking and peeling happen in the samples that are provided by Harvard University. The photoresist used for this wafer is the S1822, which is the same family as the S1813. However, the physical and chemical properties may be different which is why the carbon film could not be fabricated properly. Moreover, there are two different types of wafer used for this experiment, namely, bare silicon wafer and silicon dioxide wafer. The left hand side of figure 3 is the silicon dioxide and bare silicon wafer is on the right side. By comparing the two wafers, it may be worth mentioning that the silicon dioxide wafer seems to provide a better surface for the carbon films to adhere to the surface. Evidently from figure 3, there are less cracking and feeling on the silicon dioxide wafer than the silicon wafer.

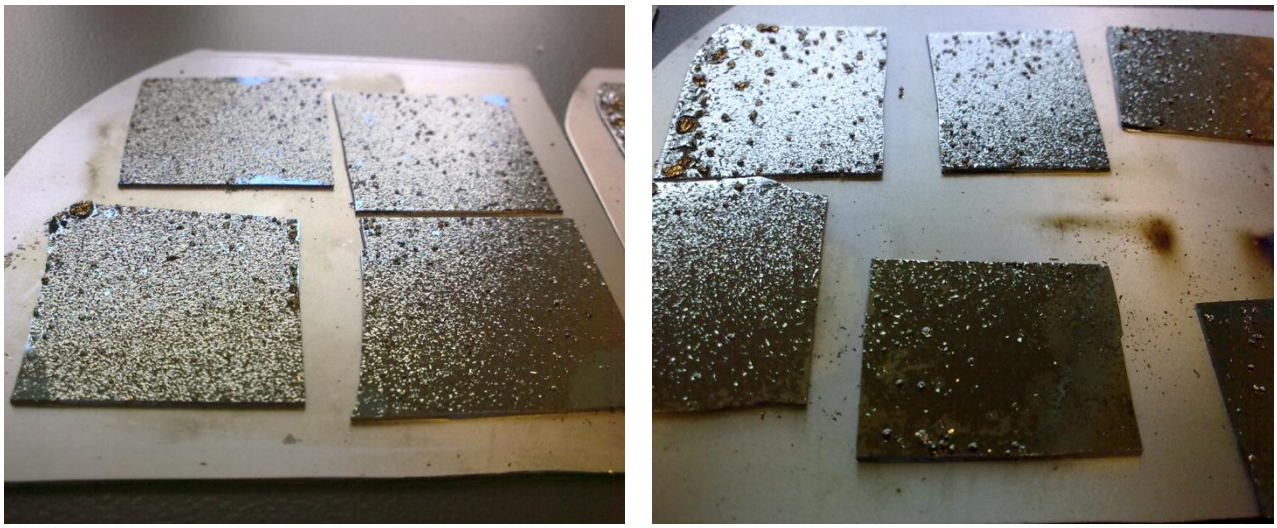

**Figure 3: Cracking and Peeling of the Carbon Film**

### 4.1.2 Method 2 Results:

Samples pyrolyzed: Carbon, Carbon+0.1ml of $Fe_3O_4$

Cracking and peeling occur after pyrolysis and the results are similar to those in method 1.

### 4.1.3 Method 3 Results:

Samples pyrolyzed: Carbon, Carbon+0.1ml of $Fe_3O_4$

The iron oxide samples turn out smooth, all of those samples are stable in water and ethanol. Four out of six samples of carbon are stable in water. Hence those are the samples that are taken for the cell adhesion test.

### 4.1.4 Method 4 Results:

Samples pyrolyzed: Carbon+0.6ml of $Fe_3O_4$, Carbon+0.5ml of Au, Carbon+3ml of Au

Figure 4 and 5 displays the result of the new wafers. The wafers used for this particular experiment is the P-type silicon wafer with an orientation of <100>. Clearly, a smooth carbon surface is formed after pyrolysis. However, when the samples are soaked with either water or ethanol, the water seems to penetrate through the film leading to the peeling of the carbon film off the silicon surface. Water and ethanol penetrate through both the iron (III) oxide samples and the gold samples as may be seen from figures 4 and 5. The major difference is that the entire carbon/iron nanoparticle film peels off the silicon surface when the samples are left to dry in air after soaking in water and ethanol. Carbon/Gold nanoparticle film on the other hand, still adhere to the surface but with lots of wrinkles on the film. The only sample that does not peel off in water or ethanol is the Carbon+3ml of Au. All of the Carbon+0.5ml of Au samples have wrinkles after being soaked in water as may be seen in figure 5. Therefore, the carbon+3ml of Au are used for cell culture.

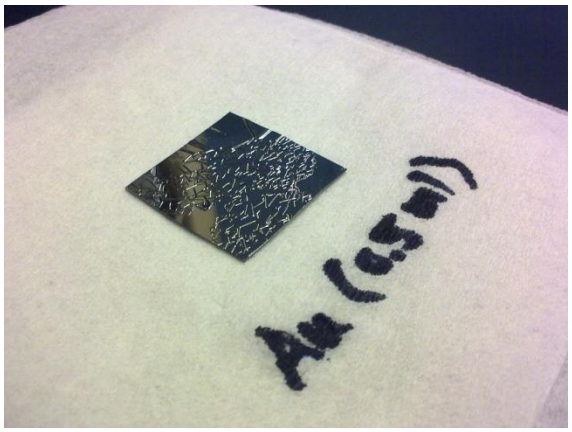


**Figure 5: Carbon/gold nanoparticle Film After Soaking in Water/ethanol**

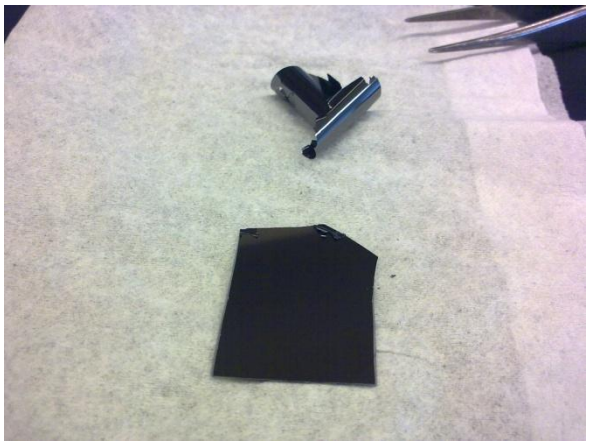

**Figure 4: Carbon/Iron (III) oxide Nanoparticle Film After Soaking in Water/ethanol**

### 4.1.5 Method 5 Results:

Samples pyrolyzed: Carbon+0.1ml of $Fe_3O_4$, Carbon+0.5ml of $Fe_3O_4$

From figure 6, this procedure does not work well. Cracking and peeling happen during the pyrolysis process. The substrate that do not crack during the pyrolysis peel off after being soaked in water for 24 hours.


**Figure 6: Pyrolysis Method 5 Results**

### 4.1.6 Method 6 Results:

Samples pyrolyzed: Carbon, Carbon+0.1ml of $Fe_3O_4$, Carbon+0.5ml of $Fe_3O_4$

**Table 2: Result from Method 6 of Pyrolysis**

| Samples | Notes |
|---|---|
| Carbon (06/18/2009) | Stable in water and ethanol |
| Carbon (06/05/2009) | Stable in water and ethanol |
| Carbon+0.1ml $Fe_3O_4$ (06/18/2009) | Stable in water and ethanol |
| Carbon+0.1ml $Fe_3O_4$ (06/05/2009) | Stable in water and ethanol |
| Carbon+0.5ml $Fe_3O_4$ (06/18/2009) | Stable in water and ethanol |
| Carbon+0.6ml $Fe_3O_4$ (06/05/2009) | Stable in water and ethanol |

*Bracket indicated the date when the samples were spin coated.

Following pyrolysis method #6, as shown in table 2, all of the pyrolyzed film appears to be stable in water and ethanol. The pyrolyzed films are also soaked in water over night to test for the strength of film adhesion to the silicon wafer. As expected, the films are still strongly attached to the silicon surface after 24-hour soaking period.

### 4.1.7 Method 7 Results:

Samples pyrolyzed: Carbon, Carbon+0.1ml of $Fe_3O_4$

As may be seen from figure 7, the samples after pyrolysis turn out well. However, when the samples are soaked in water, the $Fe_3O_4$ samples peel off completely. Water also penetrates through the carbon samples; however, the carbon film is still intact with the silicon surface after the samples are dried in air.

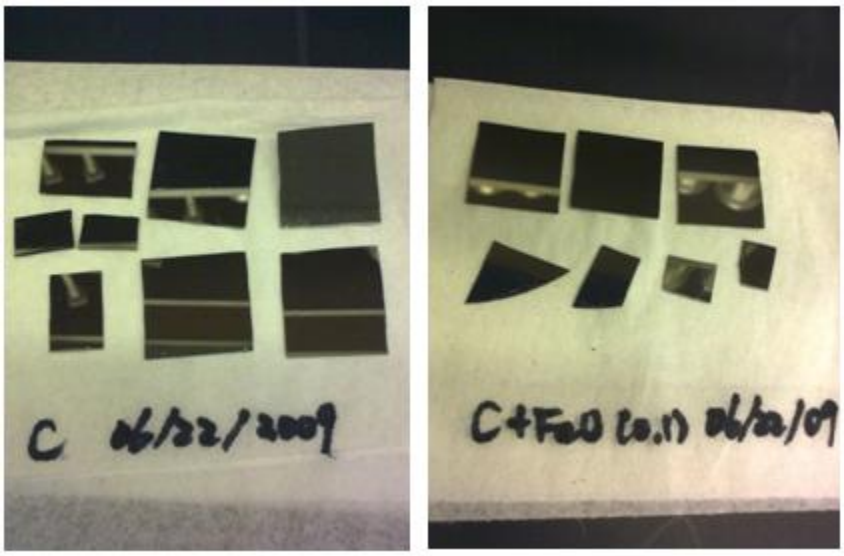


**Figure 7: Pyrolysis Method 7 Results**

### 4.1.8 Method 8 Result:

Samples pyrolyzed: Carbon, Carbon+0.1ml of $Fe_3O_4$, Carbon+0.5ml of Au Carbon+3ml of Au.

The result of method 8 is in agreement with method 7. The carbon films shows strong attachment to the silicon wafer. The pyrolyzed films are also soaked in water over night to test for the strength of film adhesion to the silicon wafer. As expected, the films are still strongly attached to the silicon surface after 24-hour soaking period

## 4.2 Cyclic Voltammetry Results:

Figure 8 shows the CV result for pyrolysis methods 3 and 7. The red line represents pyrolysis method 3 whereas the blue line represents pyrolysis method 7. Clearly, the delta E values are very similar and stable at 0.250 eV.

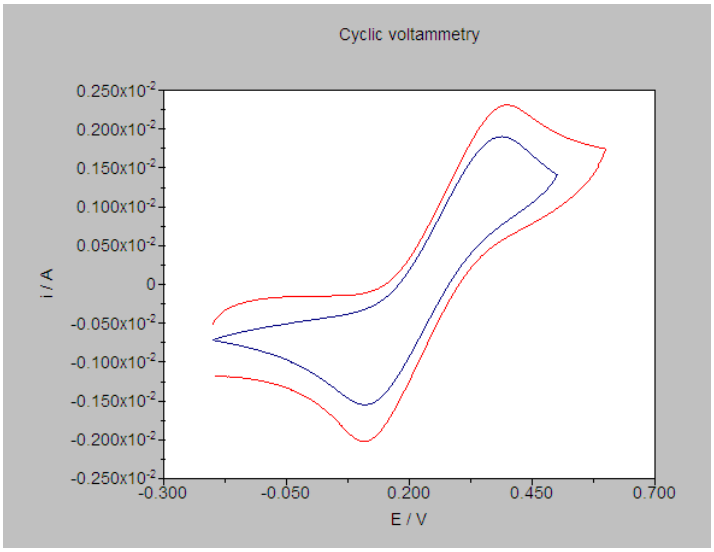


**Figure 8: CV Results for Pyrolysis Method 3(red) and 7(blue)**

Figure 9 shows the CV result of Au nanoparticle films (blue) compared to carbon (red). The delta E value for the gold nanoparticle sample is about twice as large as the bare carbon sample when pyrolyzed under the same procedure.

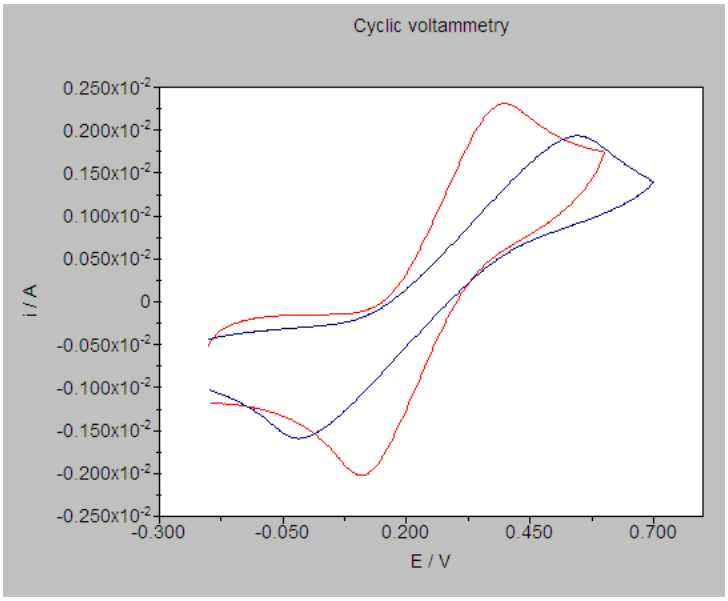


**Figure 9: CV Result of Au Nanoparticle Films (blue) Compared to Carbon (red)**

## 4.3 Film Loss Assessment

Table 3 discloses the film thickness of different substrates before and after pyrolysis

**Table 3: Film Loss Assessment Results**

| Type | Film distance (µm) | Substrate distance (µm) | Film thickness (µm) | % loss |
|---|---|---|---|---|
| Pyrolyzed S1813 (10°C/min heat rate second step) | 163.6 | 162.1 | 1.5 | |
| Unpyrolyzed S1813 (4 coats) | 131.5 | 121.4 | 10.1 | 85.10% |
| Pyrolyzed S1813 + 3ml Au(10°C/min heat rate second step) | 151.8 | 149.5 | 2.3 | |
| Unpyrolyzed S1813 (4 coats) | 149.5 | 140.4 | 9.1 | 74.70% |

A film loss of 85.1% was observed for the bare carbon sample. This is very close to the literature reported value.

## 4.4 Surface Energy Results:

A drop of DI water is added on to the surface of fabricated substrates. From figure 10, a clear trend can be observed that the contact angle decreases as there are more Au NPs on the substrate surface. The lower the contact angle means the surface is more hydrophilic. Clearly, the addition of Au NPs makes the carbon substrate more hydrophilic.

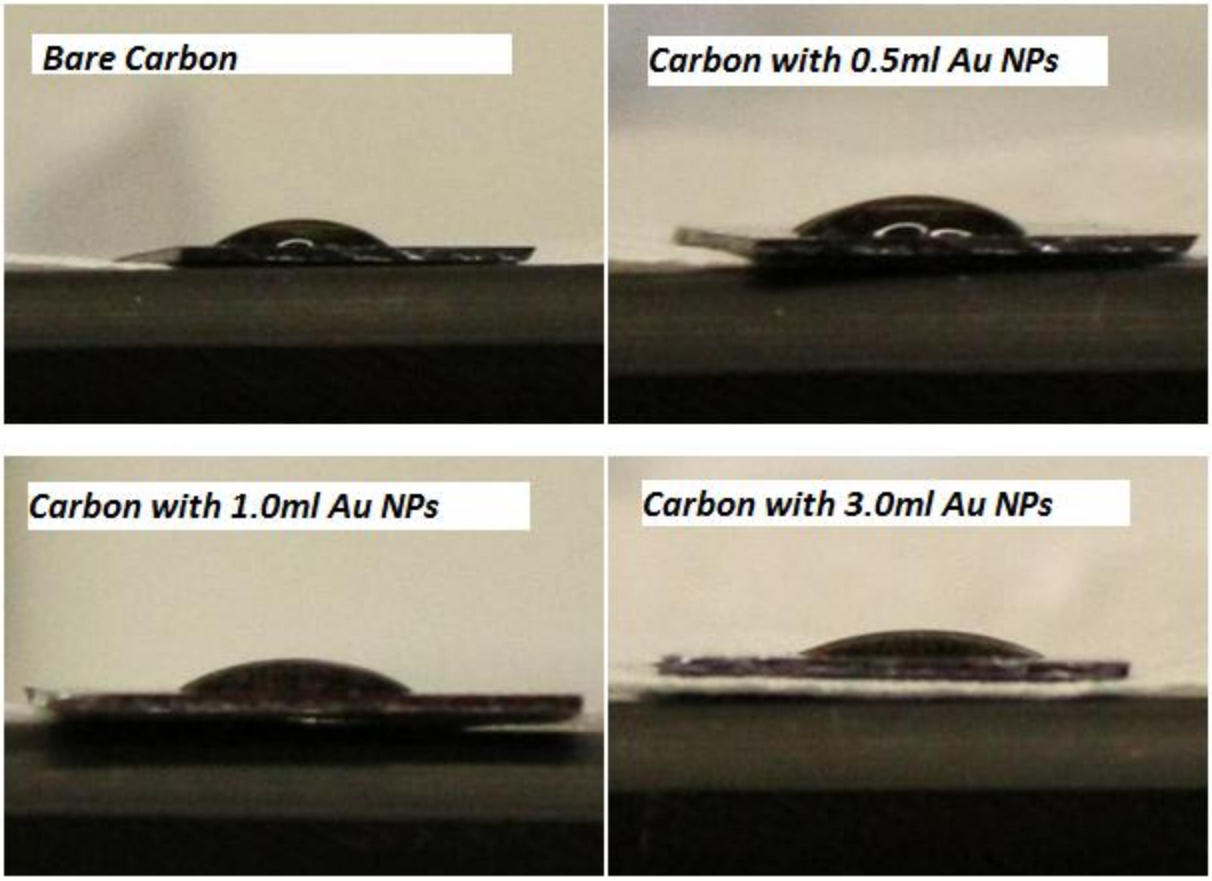


**Figure 10: Contact Angle Comparisons**

Figure 11 displays the difference in surface energy between substrates. $\gamma_{LG}$ was 72 dynes/cm for water and 58 dynes/cm for formamide. Since hexadecane does not form a contact angle, it is not included in the surface energy calculation. Bare carbon has the highest contact angle, therefore, it had the least surface energy when compared to Au NPs doped samples. Lower contact angle means higher surface energy hence showing that the Au NPs doped samples are more hydrophilic than bare carbon. Previous studies have shown that different cell types respond differently to hydrophilic or hydrophobic surfaces. However, from the cell adhesion and cell morphology assays, it is clear that PC12 cells prefers more hydrophilic surfaces because of its higher cell adhesion rate and longer neurite length. Kennedy et al. investigated on the cell response to substrates of different surface energies. They reported that lower contact angle translates to higher surface energy. In their case, the contact angle of water was used to calculate for the surface energy. However, they have reported that cells on hydrophilic surfaces take longer to double and the cell adhesion rate is lower on hydrophilic surfaces and higher on hydrophobic surfaces.

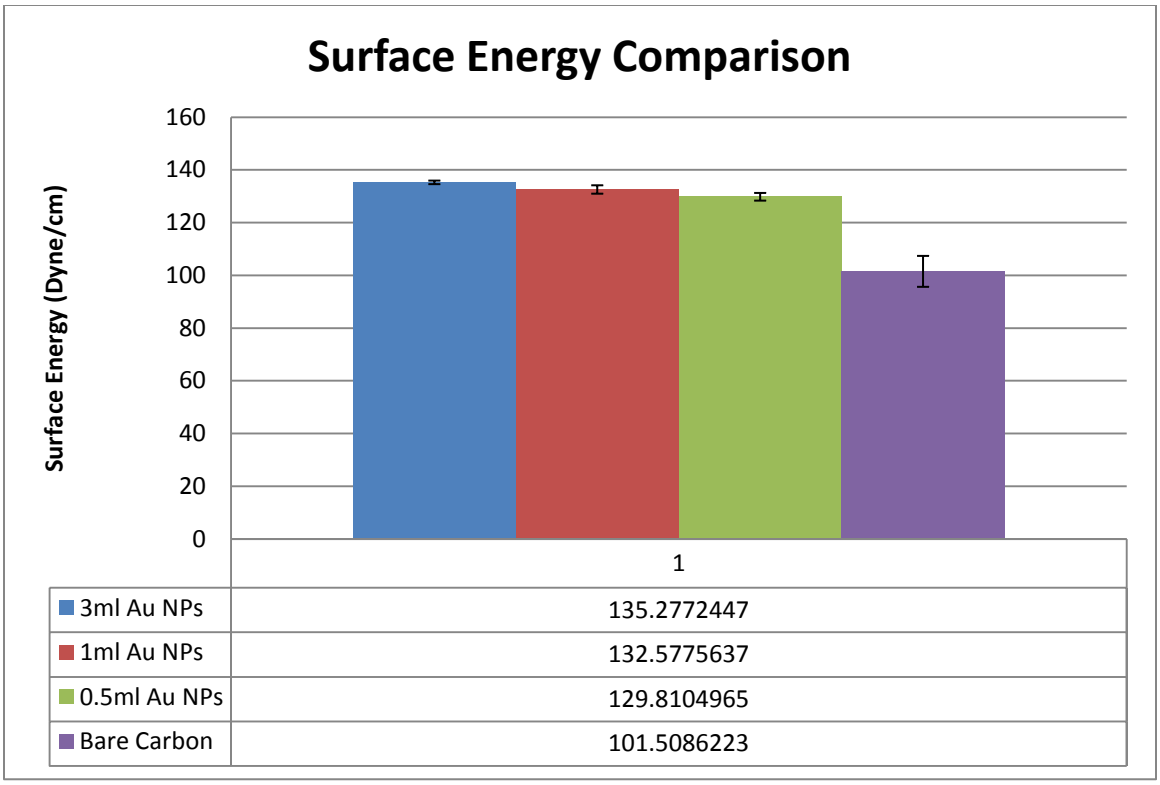


**Figure 11: Surface Energy Comparison**

## 4.5 Cell Adhesion Assay

### 4.5.1 Cell Adhesion Test Method 1:

Even though some films peel off from the silicon surface, some are still attached after soaking them in water and ethanol. Those samples are used for cell culture. Cell adhesion test is done following the procedure described previously. Figure 12 shows the difference in cell adhesion for different substrates. One major thing to notice is that all of the carbon/gold films cracked after being soaked in growth media for 3 days. Carbon and carbon/iron III oxide film appear to be still intact with the silicon surface. Figure 12 shows that by adding PL and NGF seem to change a lot of the surface chemistry of the samples. However, given the same conditions, the nanoparticle samples recover more cells than the bare carbon samples.

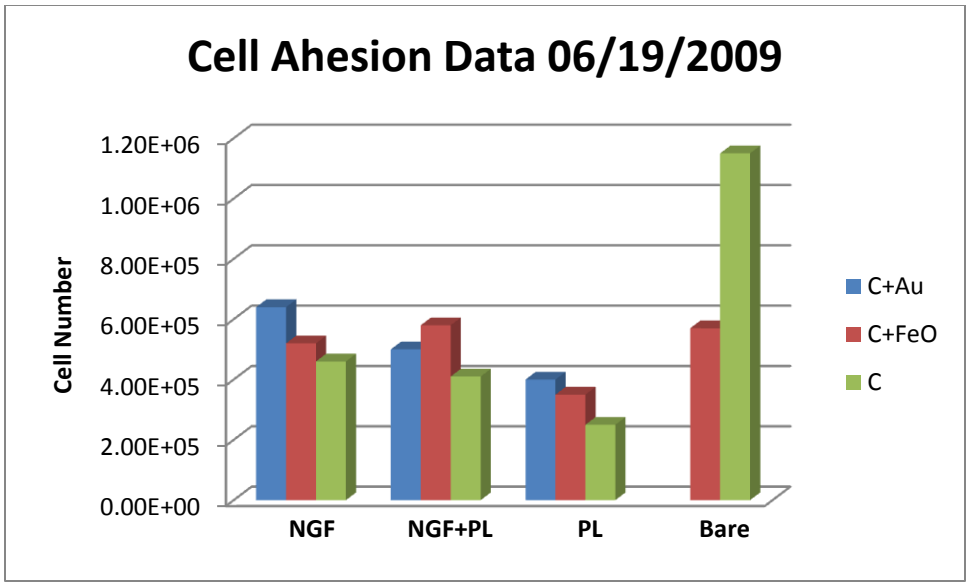


**Figure 12: Cell Adhesion Data for Different Substrates**

### 4.5.2 Cell Adhesion Test Method 2:

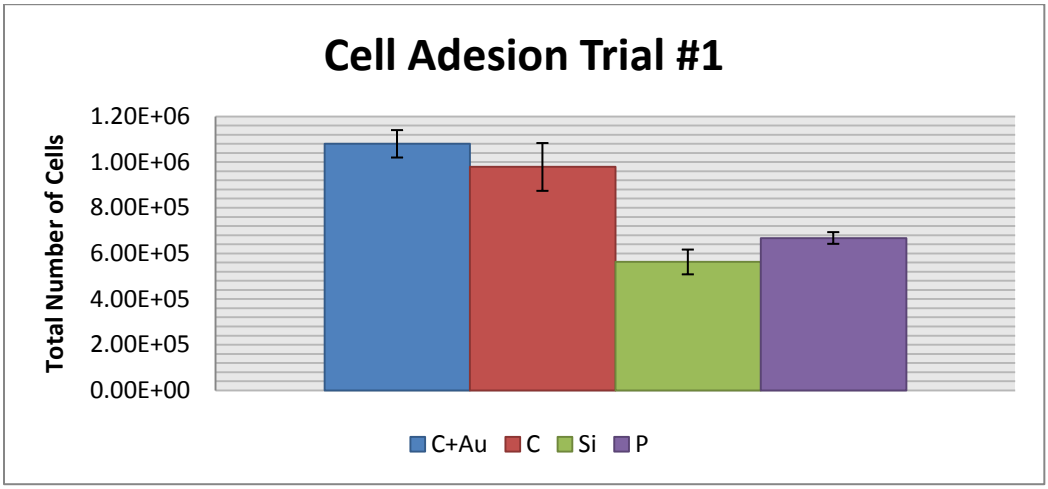


**Figure 13: Cell Adhesion Data for Different Substrates**

Poly-Lysine (PL) has shown to improve cell adhesion when coated on glass. However, the interaction between PL and carbon surfaces remains unknown. Since there is no way to detect that PL could be successfully coated on the carbon surface, the PL step from method 1 is taken out to simplify and conduct a more accurate experiment. The goal of the project is to see whether carbon is a better surface to enhance cell growth and the ability of carbon to produce even better cell growth result than PL coated glass. All of the carbon samples perform relatively well and is better than PL coated glass as may be seen from figure 13. Lack of difference can be seen between the C and C+Au samples. Figure 14 is another set of cell adhesion data. Similar to trial one, all of the carbon films are still attached to the silicon wafer even when soaked in growth media for 24 hours which shows the pyrolysis procedure is consistent and reliable. By comparing figure 14 to figure 13, a very similar trend can be concluded. The

carbon samples clearly perform much better than the silicon and plastic. From the uncertainty bars, it is almost certain that Au NPs doped carbon sample performs slightly better than the bare carbon sample.

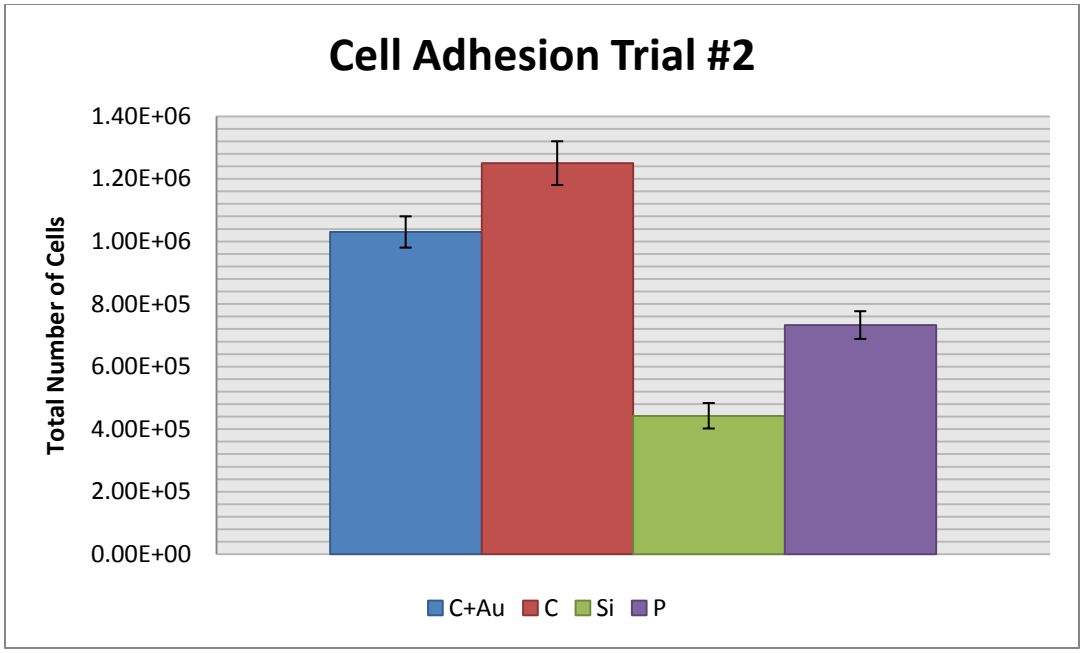


**Figure 14: Cell Adhesion Data for Different Substrates**

Another interesting thing to notice is that cells have already proliferated after one day of cell culture.

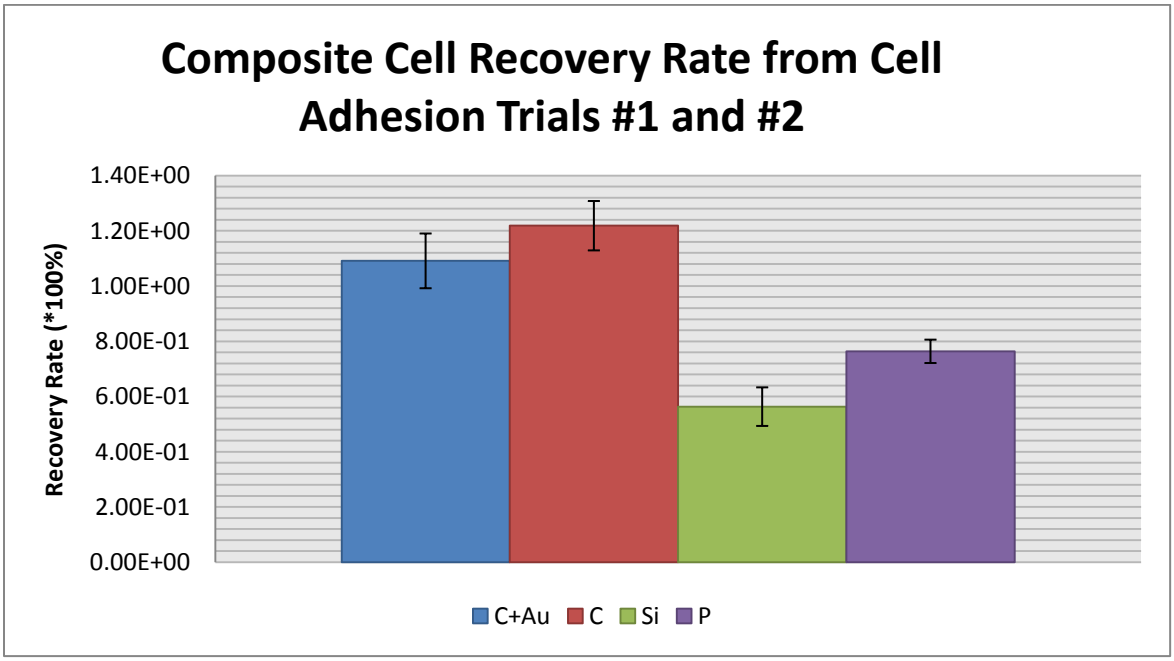


**Figure 15: Cell Recovery Rate of Different Substrates**

From figure 15, the cells proliferate on the bare carbon and Au NPs doped carbon. The recovery rates for all of the bare carbon and Au NPs doped carbon are twice as much when compared to silicon and glass,

which means that carbon and Au NPs doped carbon are much better substratum for cells to grow and proliferate.

Figure 16 and 17 show the difference in cell adhesion and cell recovery rate for carbon samples of different gold nanoparticle concentrations.

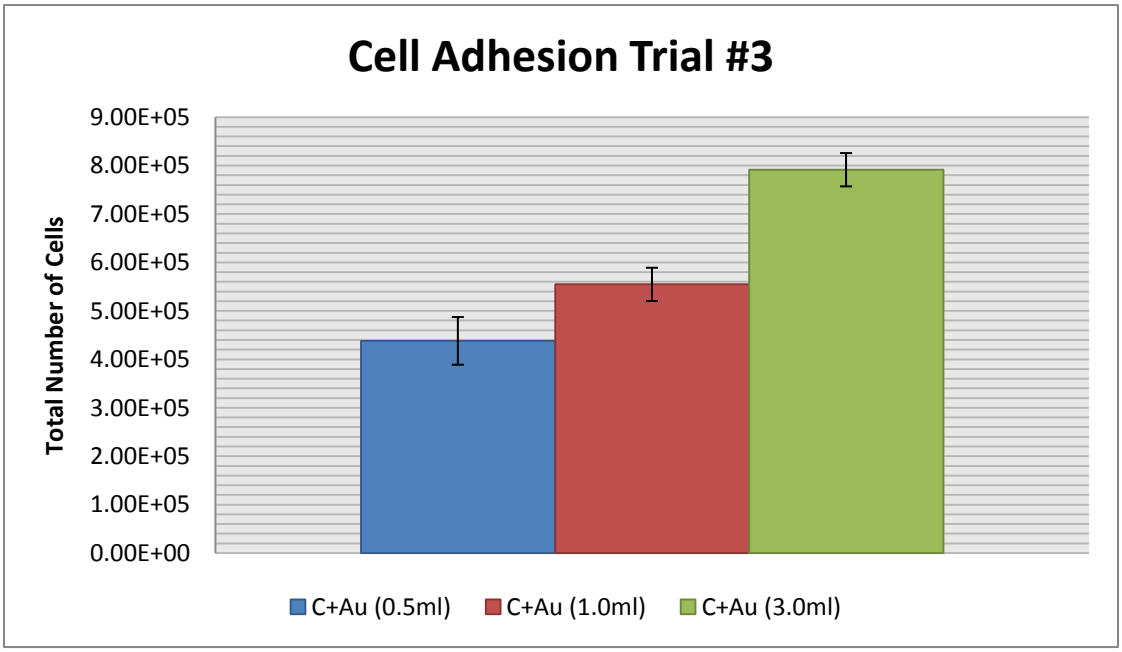


**Figure 16: Adhesion Data for Gold Nanoparticles of Different Concentrations**

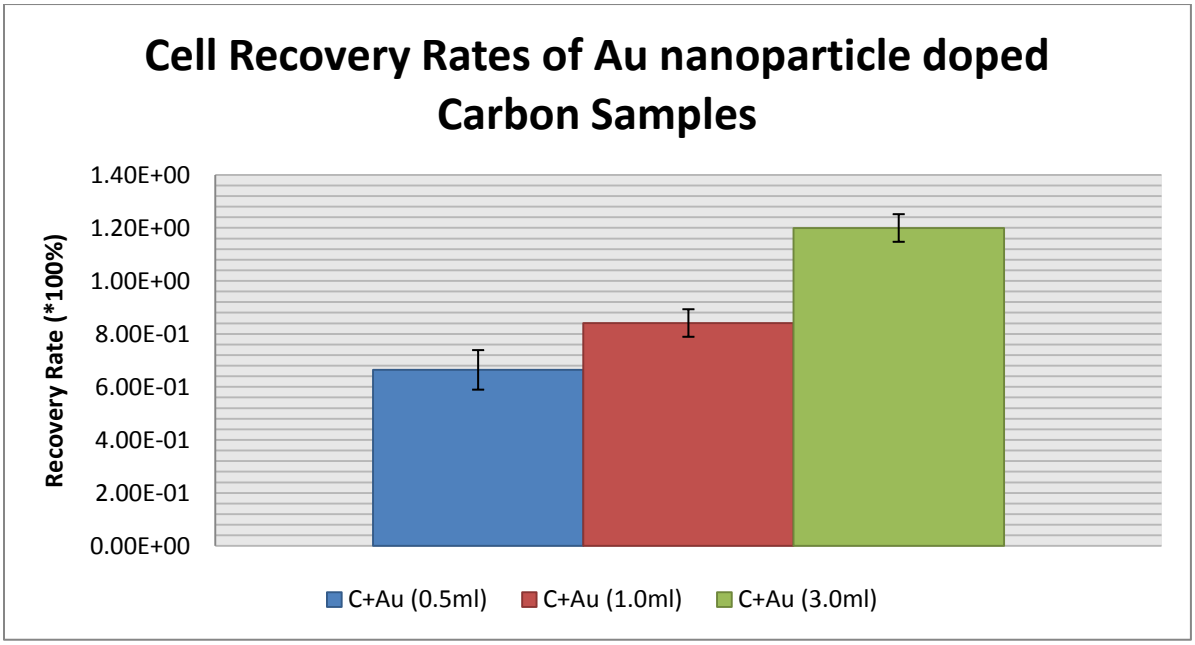


**Figure 17: Cell Recovery Rates for Gold Nanoparticles of Different Concentrations**

Clearly, samples with higher concentration of gold nanoparticles have a higher cell adhesion and cell recovery rates. It is assumed that higher gold nanoparticle concentration makes the surface rougher and increases the overall surface energy, thus making the cells easier to attach to the substrate.

## 4.6 Cell Morphology Assay:

### 4.6.1 Cell Morphology Assay Trial #2:

Interesting observation is found that cells on carbon surface are still able to differentiate even without the presence of Nerve Growth Factor (NGF) as may be seen in figure 18.

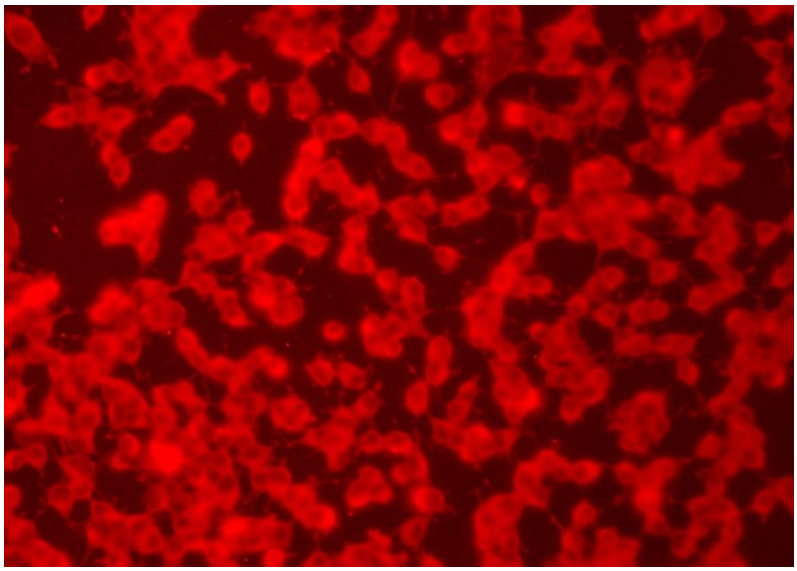

**Figure 18: Differentiation of Cells on Carbon Surface without the Presence of NGF**

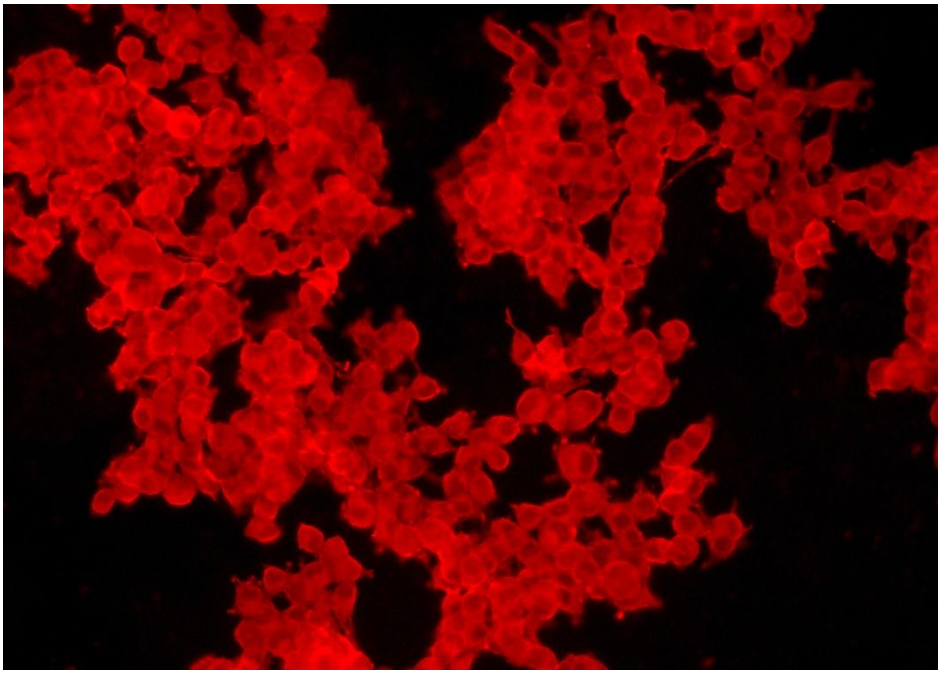

**Figure 19: Cells on PL Coated Glass Samples**

By comparing figure 19 to figure 18, carbon out-performs PL coated glass because the cells have differentiated better (i.e. neurite length) on the carbon surfaces.

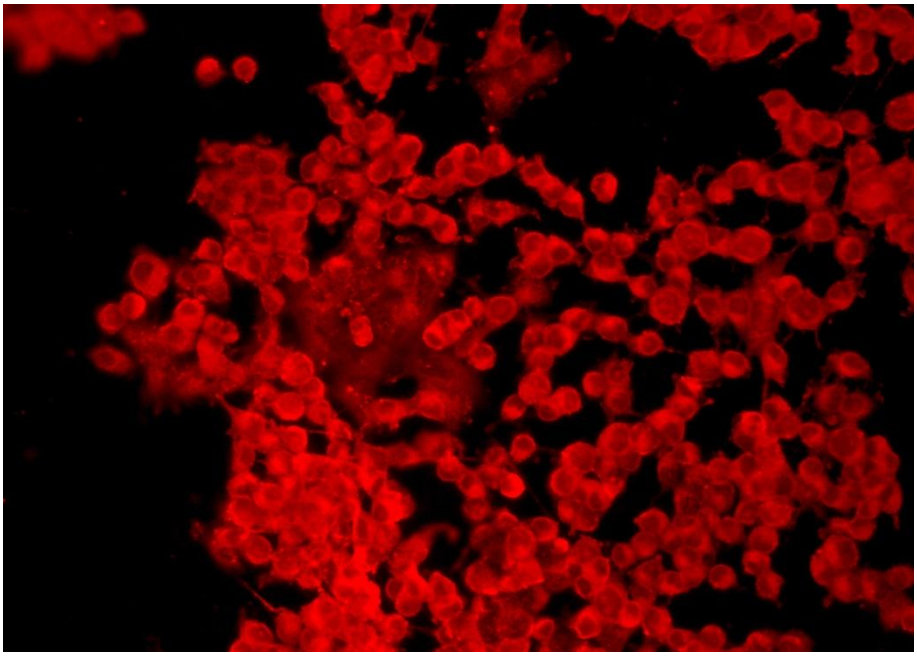

**Figure 20: Cells on Carbon with Gold Nanoparticles Surfaces**

Figure 24 and 25 pretty much summarized the length of neuritis for different substrates.

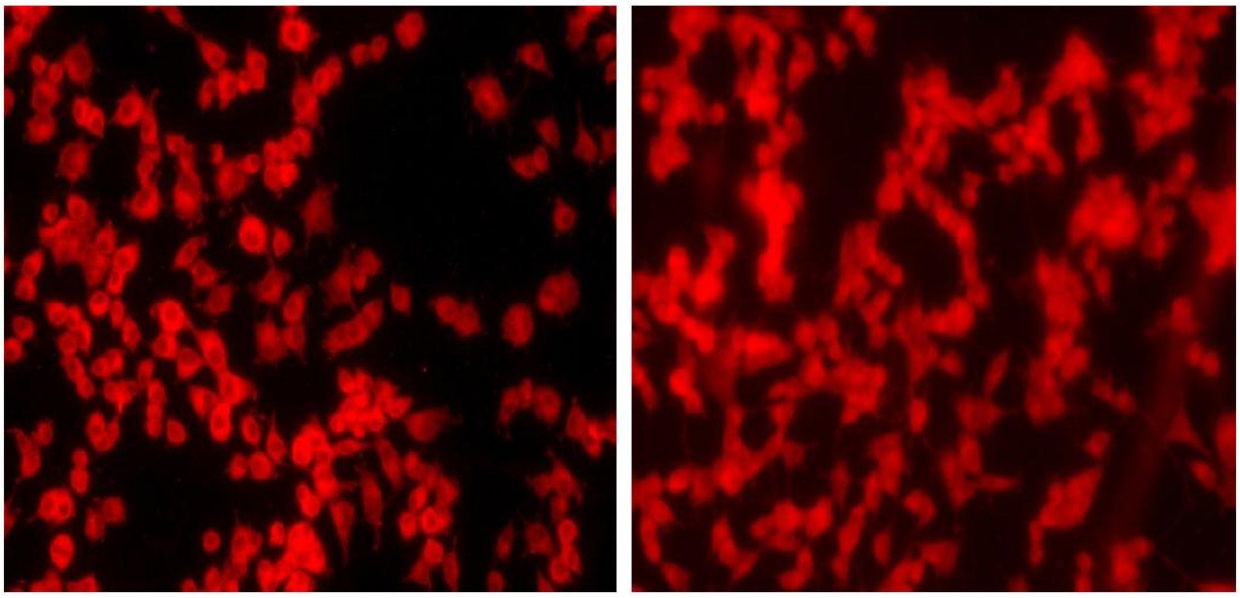


**Figure 21: The Effect of NGF on Carbon Substrates**

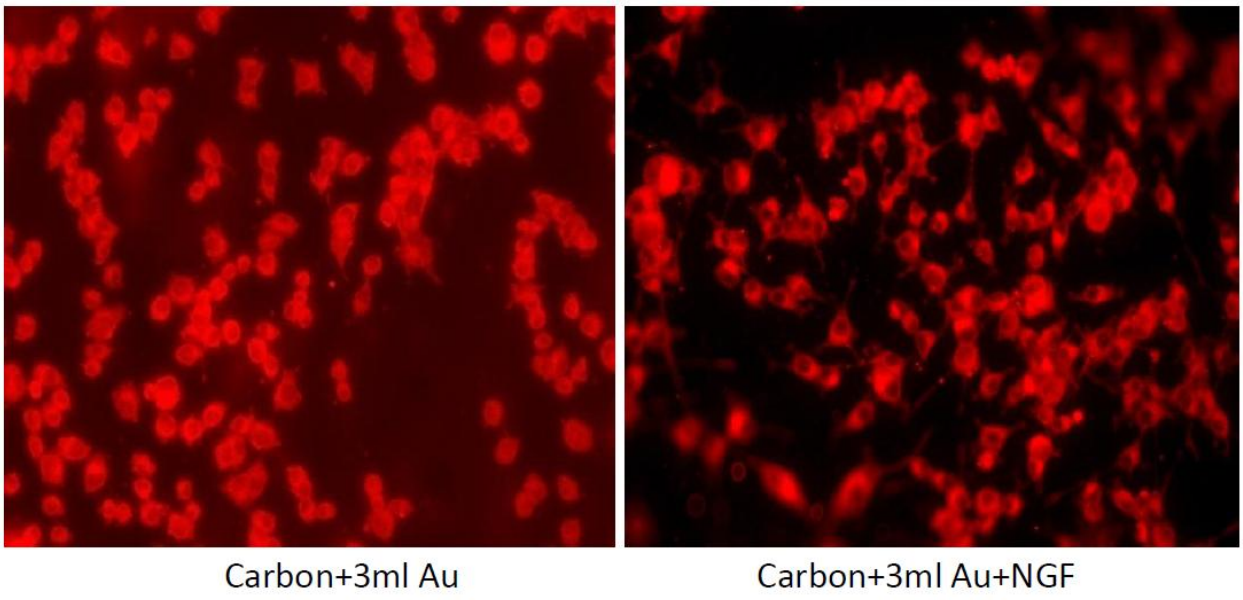


**Figure 22: The Effect of NGF on Carbon+Au NPs Substrates**

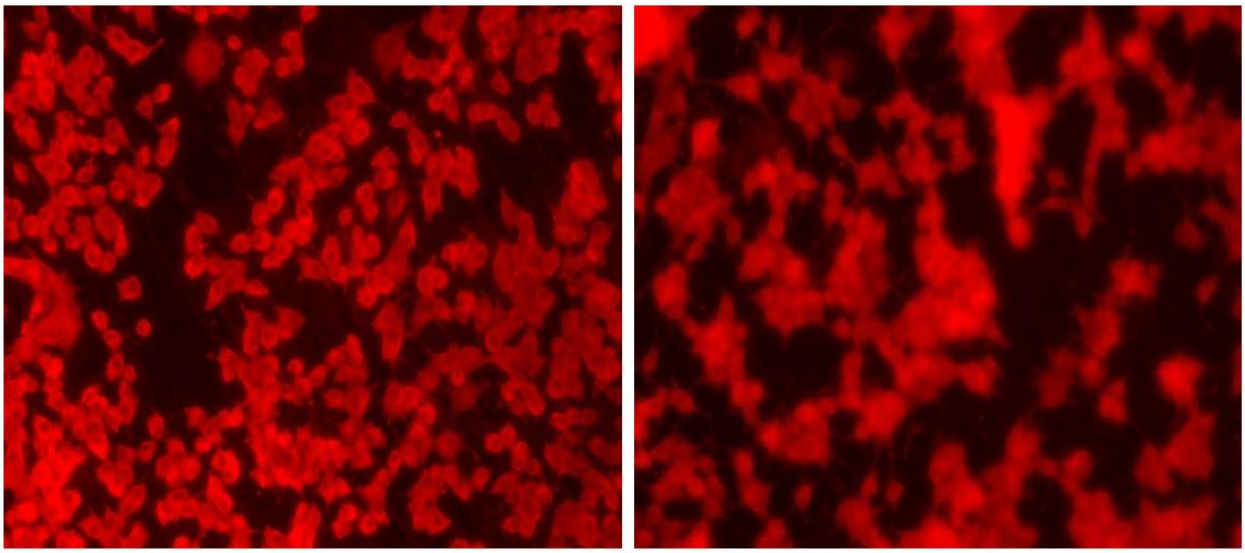


**Figure 23: The Effect of NGF on PL Coated Glass**

Figure 21 to 23 show the effect of NGF once it is applied to the substrates. These qualitative results are quantified into figure 24 through 27. One aspect of the pictures that is not taken into account is the amount of clusters. Due to the application of Poly- Lysine on the glass substrates, a lot more cells are visible than the carbon and carbon+Au substrates. As more cells are present, a lot more clusters are formed for the glass sample.

After the application of NGF, the cellular morphology of the glass and bare carbon samples change from circular to more irregular shapes. However, for the Au NPs sample, the cells remain in circular shape with visible nucleus. From the previous studies, it is well evident that the application of gold nanoparticles greatly affects the cellular morphology. In our case, the surface tension provided by the gold nanoparticles prevents the cells from spreading. This result can be correlated to figure 27, where the Au NPs sample has the lowest cell body area when compared to other substrates.

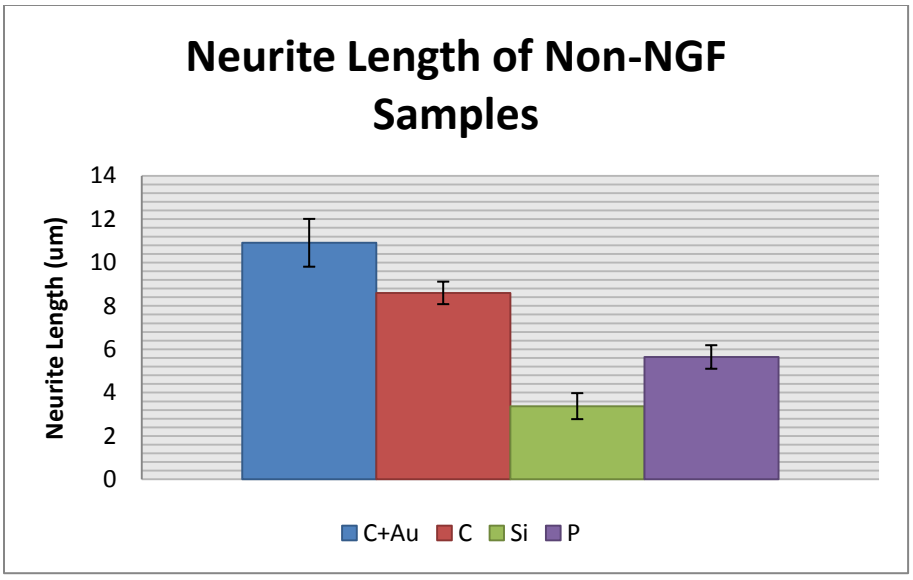


**Figure 24: Neurite Length for Non-NGF Samples**

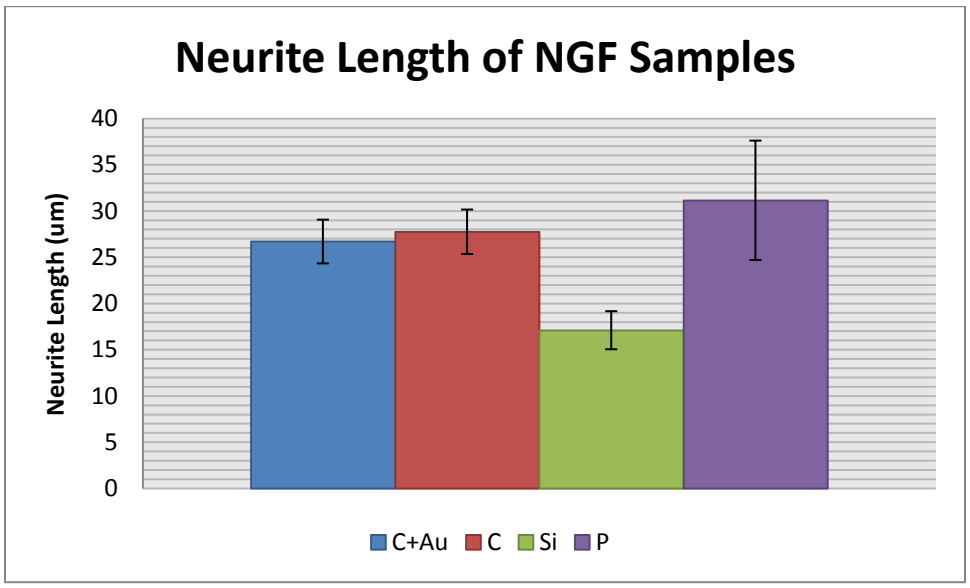


**Figure 25: Neurite Length for NGF Samples**

The longer the neurite, the better the substrate for neuronal growth. For the non-NGF samples, gold nanoparticles doped samples clearly have the longest neurite. However, when uncertainty is taken into account, bare carbon also has comparable lengths to gold nanoparticle doped samples. This could be said that nanoparticle doped samples are rougher than the others, thus enhancing neurite extension. When NGF is added, very interesting effect happens on the PL coated glass sample. Even though it has the longest neurite when NGF is applied, the uncertainty is huge when compared to other samples.

Cell body area is also another indicator for neuronal growth. Figure 26 and 27 explain the difference in cell body area for different substrates. Without the presence of NGF, bare carbon, bare silicon and carbon+Au samples show very similar cell body area, indicating that all three of them are ideal for cell

growth. However, once the NGF is applied, the gold samples show the lowest cell body area. This is understandable because the presence of gold nanoparticle does indeed influence the shape of cells. With the uncertainties taken into account, plastic, silicon and carbon all show very similar cell body area after the application of the NGF.

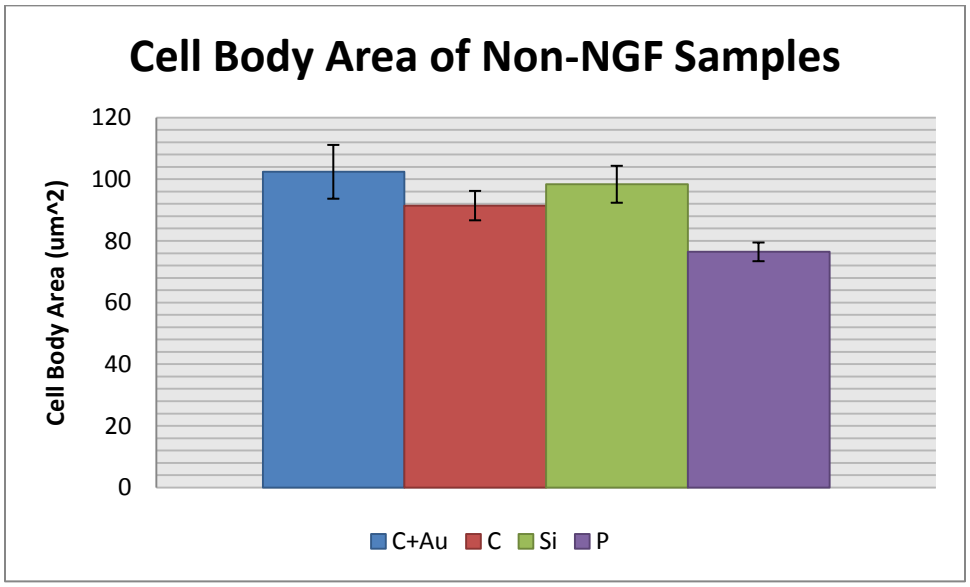


**Figure 26: Cell Body Area of Non-NGF Samples**

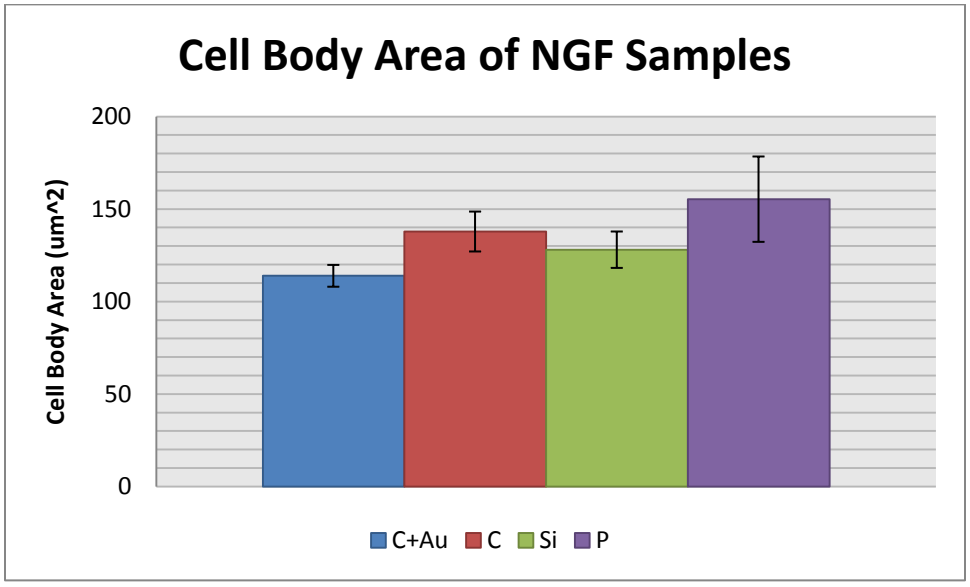


**Figure 27: Cell Body Area of NGF Samples**

### 4.6.2 Cell Morphology Assay Trial #2:

Another cell morphology assay is done to prove that the result obtained from trial #1 is reproducible. Clearly, they show very similar trend in neurite length as shown in figure 28 and 29. As expected from trial #1, the carbon with gold nanoparticles samples have longer neurite length than the bare carbon

samples. However, by comparing it to trial #1, the addition of Poly-Lysine to glass sample seems to have shorten its neurite when the NGF is applied. One important aspect is that the average neurite length of all the carbon samples have been consistent in both trial 1 and 2 (10.5um for Au samples and 8.1um for bare carbon samples).

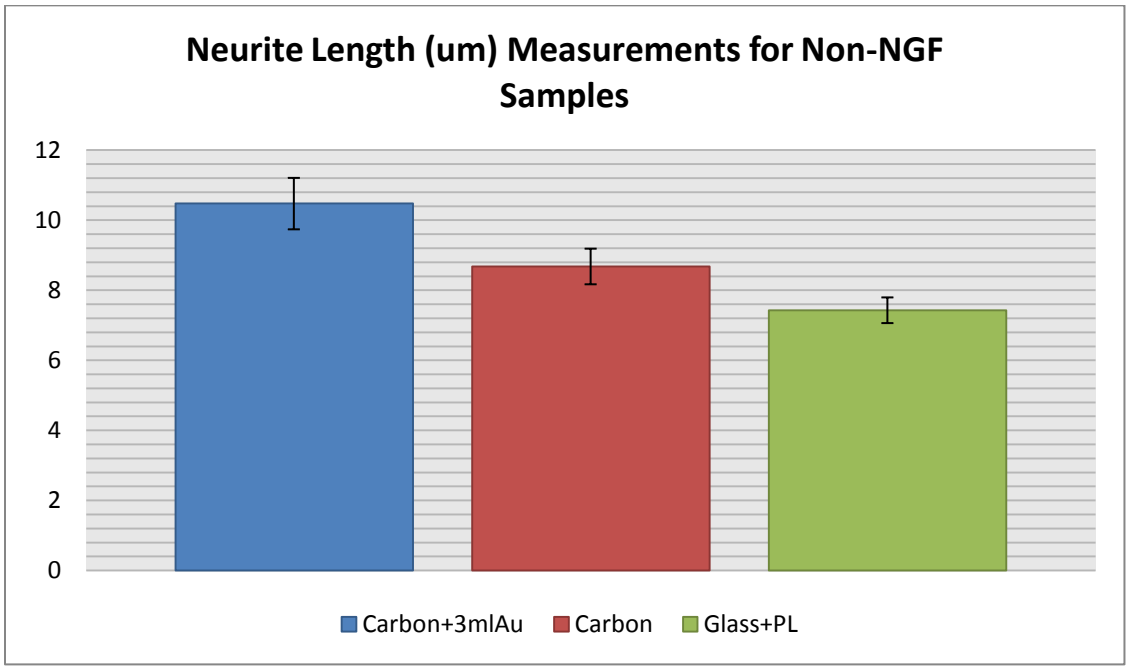


**Figure 28: Neurite Length for Non-NGF Samples**

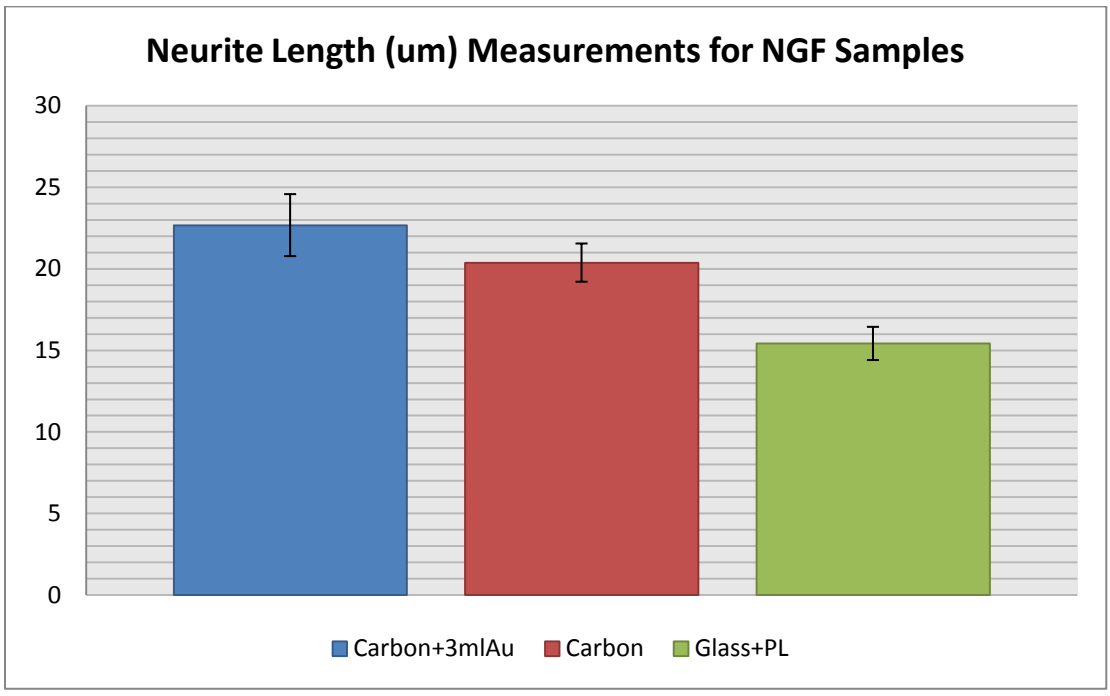


**Figure 29: Neurite Length for NGF Samples**

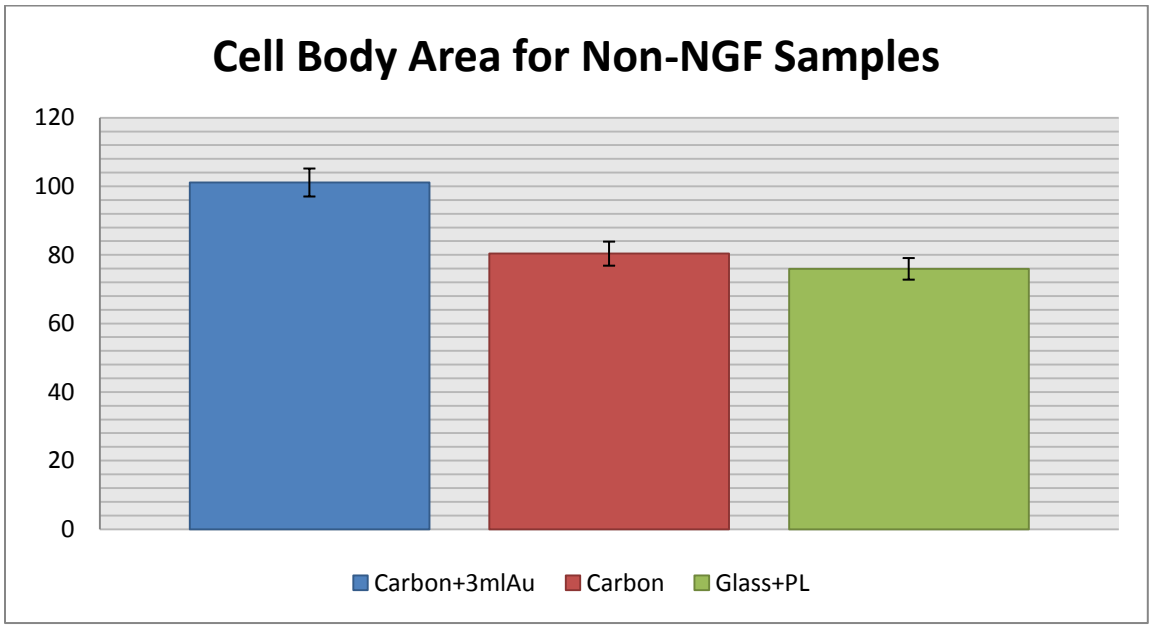


**Figure 30: Cell Body Area for Non-NGF Samples**

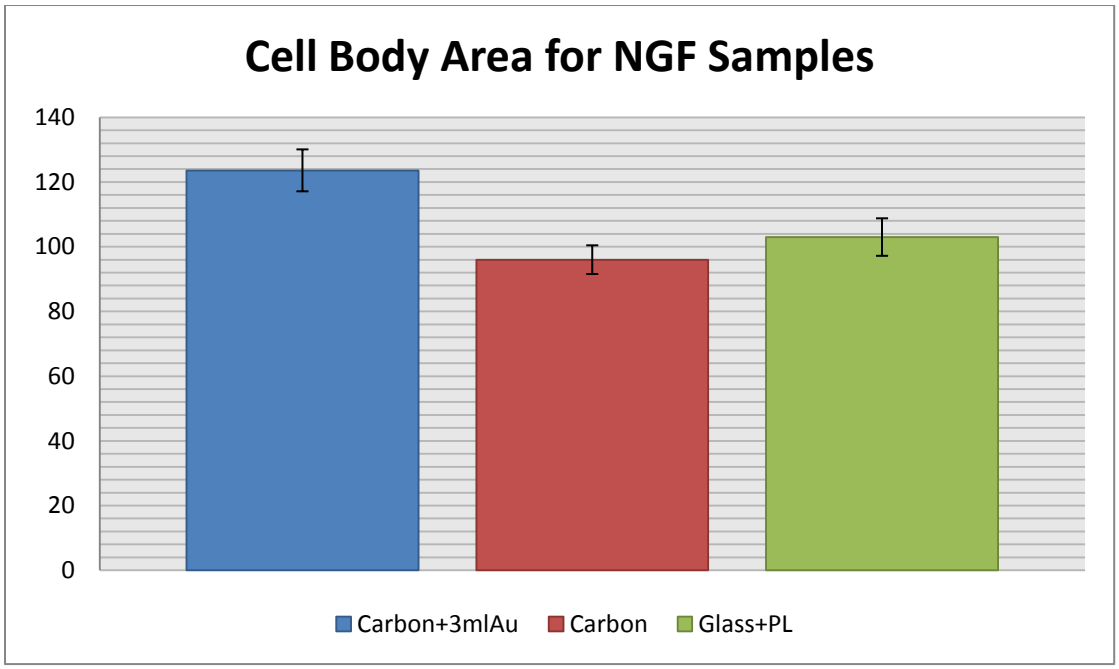


**Figure 31: Cell Body Area for NGF Samples**

### 4.6.3 Cell Morphology Assay for gold samples of different concentrations:

The neurite length of gold samples of different concentrations is also being measured. From figure 32, it could be easily said that the neurites tend to extend longer at higher gold nanoparticle concentrations. Figure 32 also sets a very good correlation with figure 28. The bare carbon sample in figure 28 has a length at about 8um. From figure 32, at 0.5ml Au, the average neurite length is slightly longer than the bare carbon sample. Same trend can be observed as the concentration is increased. This result proves that the hypothesis is valid. Presumably, as gold nanoparticle concentration increases, the surface will be rougher making the neurites to extend longer as Fan et al. have proven previously.

The qualitative results of gold samples of different concentrations could be found in the Appendix. The NGF+carbon+ 3ml Au cell culture was contaminated and as a result of that, no pictures were taken. From figures 35-37, a comparison could be drawn in terms of the cell body area. As more Au NPs were added to the carbon substrate, the surface tension of the substrate increases, leading to lower individual cell body area.

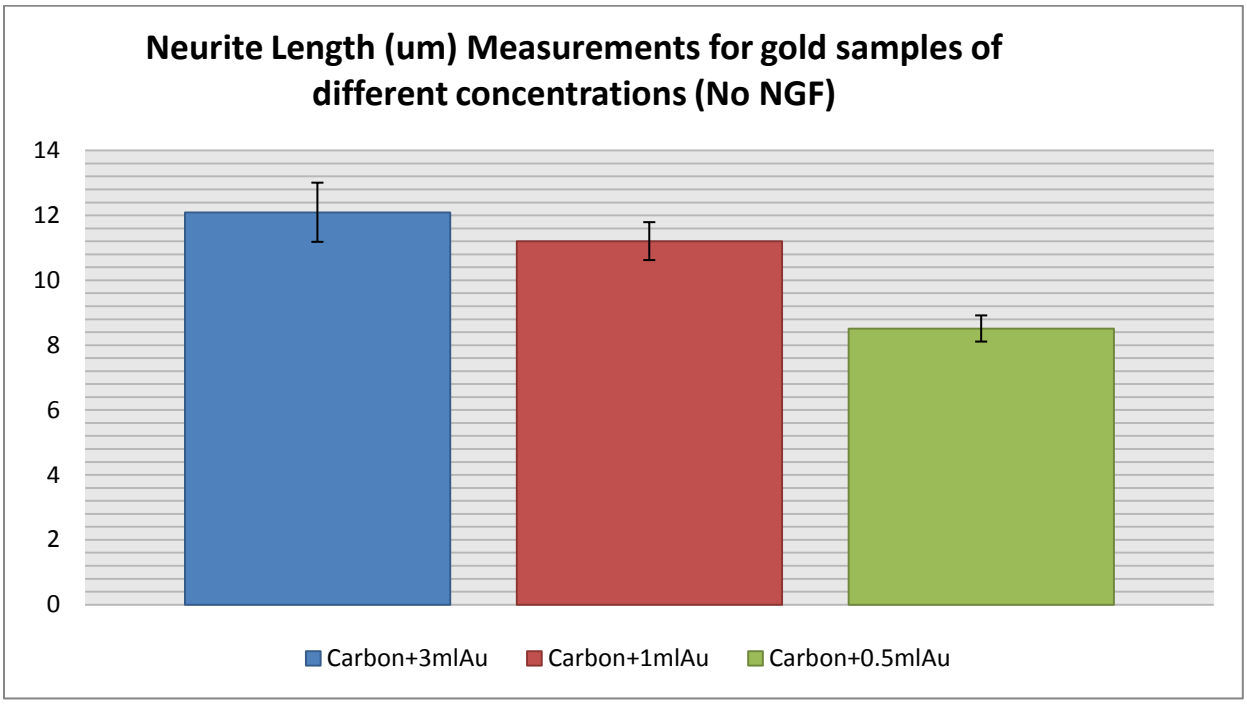


**Figure 32: Neurite Length for Gold Samples of Different Concentrations**

## 4.7 Atomic Force Microscopy

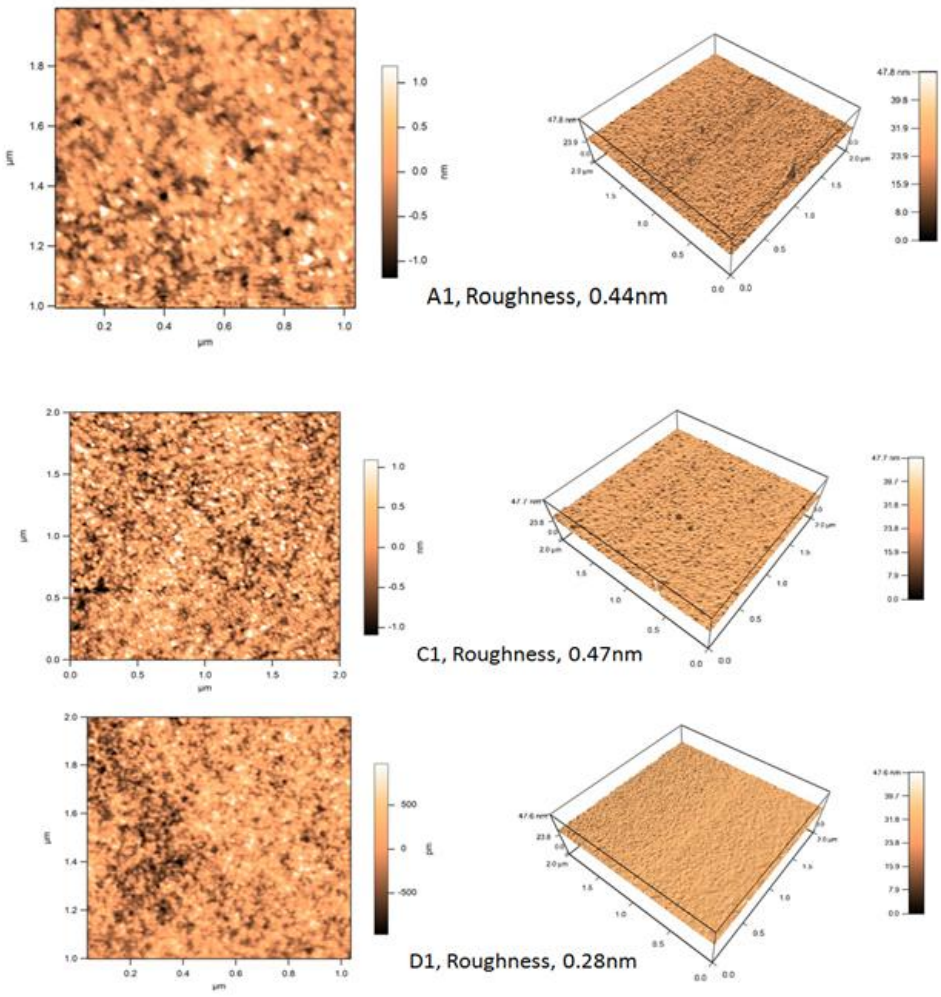


**Figure 33: AFM Images of Bare Carbon (A1), 0.5ml Au (C1) and 3ml Au (D1)**

Figure 33 shows the AFM images of different substrates. The roughness does not have a direct relationship with the concentration of Au NPs. As shown in previous studies, Hallab et al. concluded that the influence of surface roughness upon cell adhesion strength may be secondary to surface energy on high energy substrates. Their experiments led to the final conclusion in figure 34. As surface energy increases, its effects on cellular adhesion strength increases. Roughness on the other hand, has an opposite relationship. Additionally, it was reported by Fan et al. that Nigra cells can adhere well on the surface with an average roughness in the range of 20-70 nm. It was also shown that higher roughness will lead to lower cell proliferation by Ponsonnet et al. However, in their studies, the roughness was between 500nm and 7um. By comparing it to the measured roughness of 0.47nm, surface roughness does not seem to play a role in cell adhesion or cell differentiation simply because the surface roughness is too small to even have any effects.

Further investigation is done to the surface roughness. Due to the inability to actually pattern the substrate, the roughness at each point of the substrate is different from one another. Typical range of roughness is between 0.2nm to 0.8nm. Even though the substrate has various roughness at different area of the substrate, the range of the roughness is still too small to be a factor in cell interactions with the substrate.

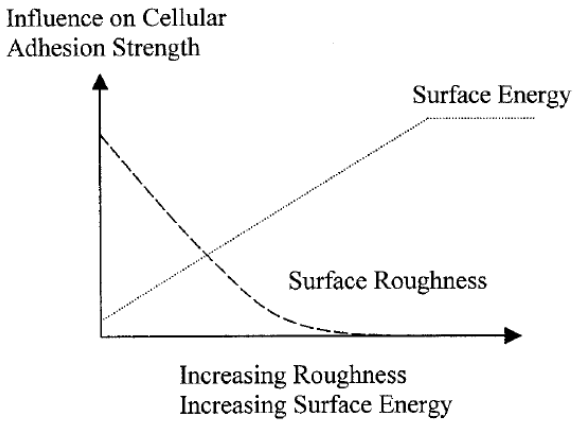


**Figure 34: Schematic Relationship between Surface Roughness, Surface Energy, and Their Respective Influence on Cellular Adhesion Strength (Hallab et al.)**

## 5. Conclusion:

In conclusion, the character of the photoresist-derived carbon film could be easily adjusted by doping different concentrations of Au NPs. The surface energy assay and AFM results show that the roughness and surface energy of the substrate are altered when different concentrations of Au NPs are doped onto the surface. The cellular adhesion result shows that carbon overall is a better substrate for nerve cell growth and differentiation than the Poly-Lysine coated glass. Increasing the Au NPs concentration increases the number of cells attached. Overall, the number of cells attached to the carbon samples are doubled compared with the amount of cells that are attached to glass. The cell morphology assays prove an important point that PC12 cells are able to differentiate without the presence of the nerve growth factor. This result shows that photoresist-derived Au NPs doped carbon films provide an ideal substratum for nerve cell culture and further work on primary neuron and stem cell will enlighten the use of Au NPs doped carbon for biomedical applications.

## Works Cited

1. Fan YW, Cui FZ, Chen LN, Zhai Y, Xu QY, Lee IS. Adhesion of neural cells on silicon wafer with nano-topographic surface. Applied Surface Science 2002;187(3-4):313-318.

2. Fukata Y, Kimura T, Kaibuchi K. Axon specification in hippocampal neurons. Neuroscience Research 2002;43(4):305-315.

3. Galobardes F, Wang C, Madou M. Investigation on the solid electrolyte interface formed on pyrolyzed photoresist carbon anodes for C-MEMS lithium-ion batteries. 2006: Elsevier Science Sa; 2006. p. 1930-1934.

4. Ghosh P, Han G, De M, Kim CK, Rotello VM. Gold nanoparticles in delivery applications. Advanced Drug Delivery Reviews 2008;60(11):1307-1315.

5. Huang HH, Ho CT, Lee TH, Lee TL, Liao KK, Chen FL. Effect of surface roughness of ground titanium on initial cell adhesion. Biomolecular Engineering 2004;21(3-5):93-97.

6. Kamei K, Mukai Y, Kojima H, Yoshikawa T, Yoshikawa M, Kiyohara G, et al. Direct cell entry of gold/iron-oxide magnetic nanoparticles in adenovirus mediated gene delivery. Biomaterials 2009;30(9):1809-1814.

7. Kim J, Song X, Kinoshita K, Madou M, White B. Electrochemical studies of carbon films from pyrolyzed photoresist. Journal of the Electrochemical Society 1998;145(7):2314-2319.

8. Malladi K, Wang CL, Madou M. Fabrication of suspended carbon microstructures by e-beam writer and pyrolysis. Carbon 2006;44(13):2602-2607.

9. Mao ZW, Wang B, Ma L, Gao C, Shen JC. The influence of polycaprolactone coating on the internalization and cytotoxicity of gold nanoparticles. Nanomedicine-Nanotechnology Biology and Medicine 2007;3(3):215-223.

10. Moriuchi T, Morishima K, Furukawa Y. Improved power capability with pyrolyzed carbon electrodes in micro direct photosynthetic/metabolic bio-fuel cell. International Journal of Precision Engineering and Manufacturing 2008;9(2):23-27.

11. Ohuchi T, Maruoka S, Sakudo A, Arai T. Assay-based quantitative analysis of PC12 cell differentiation. Journal of Neuroscience Methods 2002;118(1):1-8.

12. Panyala NR, Pena-Mendez EM, Havel J. Gold and nano-gold in medicine: overview, toxicology and perspectives. Journal of Applied Biomedicine 2009;7(2):75-91.

13. Park BY, Taherabadi L, Wang CL, Zoval J, Madou MJ. Electrical properties and shrinkage of carbonized photoresist films and the implications for carbon microelectromechanical systems devices in conductive media. Journal of the Electrochemical Society 2005;152(12):J136-J143.

14. Patra HK, Banerjee S, Chaudhuri U, Lahiri P, Dasgupta AK. Cell selective response to gold nanoparticles. Nanomedicine-Nanotechnology Biology and Medicine 2007;3(2):111-119.

15. Patra HK, Banerjee S, Chaudhuri U, Lahiri P, Dasgupta AK. Cell selective response to gold nanoparticles. Nanomedicine-Nanotechnology Biology and Medicine 2007;3(2):111-119.

16. Ponsonnet L, Comte V, Othmane A, Lagneau C, Charbonnier M, Lissac M, et al. Effect of surface topography and chemistry on adhesion, orientation and growth of fibroblasts on nickel-titanium substrates. 2002: Elsevier Science Bv; 2002. p. 157-165.

17. Ponsonnet L, Reybier K, Jaffrezic N, Comte V, Lagneau C, Lissac M, et al. Relationship between surface properties (roughness, wettability) of titanium and titanium alloys and cell behaviour. Materials Science & Engineering C-Biomimetic and Supramolecular Systems 2003;23(4):551-560.

18. Ranganathan S, McCreery R, Majji SM, Madou M. Photoresist-derived carbon for microelectromechanical systems and electrochemical applications. Journal of the Electrochemical Society 2000;147(1):277-282.

19. Sharma CS, Kulkarni MM, Sharma A, Madou M. Synthesis of carbon xerogel particles and fractal-like structures. Chemical Engineering Science 2009;64(7):1536-1543.

20. Singh A, Jayaram J, Madou M, Akbar S. Pyrolysis of negative photoresists to fabricate carbon structures for microelectromechanical systems and electrochemical applications. Journal of the Electrochemical Society 2002;149(3):E78-E83.

21. Teixidor GT, Gorkin RA, Tripathi PP, Bisht GS, Kulkarni M, Maiti TK, et al. Carbon microelectromechanical systems as a substratum for cell growth. Biomedical Materials 2008;3(3):8.

22. Teixidor GT, Zaouk RB, Park BY, Madou MJ. Fabrication and characterization of three-dimensional carbon electrodes for lithium-ion batteries. Journal of Power Sources 2008;183(2):730-740.

23. Tran DN, Ota LC, Jacobson JD, Patton WC, Chan PJ. Influence of nanoparticles on morphological differentiation of mouse embryonic stem cells. Fertility and Sterility 2007;87(4):965-970.

24. Wang CL, Jia GY, Taherabadi LH, Madou MJ. A novel method for the fabrication of high-aspect ratio C-MEMS structures. Journal of Microelectromechanical Systems 2005;14(2):348-358.

25. Wang CL, Zaouk R, Madou M. Local chemical vapor deposition of carbon nanofibers from photoresist. Carbon 2006;44(14):3073-3077.

26. Wei XL, Mo ZH, Li B, Wei JM. Disruption of HepG2 cell adhesion by gold nanoparticle and Paclitaxel disclosed by in situ QCM measurement. Colloids and Surfaces B-Biointerfaces 2007;59(1):100-104.

27. http://www.cpeo.org/techtree/ttdescript/pyrols.htm

28. Meyer, Atomic Force Microscopy, Progress in Surface Science, Vol. 41, pp, 3-49, 1992

29. Alemdaroglu et al. *Cellular uptake of DNA block copolymer micelles with different shapes*, Macromolecular Journals, (2008) 29, 326-329

30 Huang et al. *The effect of the shape of meoporous silica nanoparticles on cellular uptake and cell function*, Biomaterials xxx (2009) 1-11.

# Appendix:

**Table 4: Cell Adhesion Trial 1 (Method 2)**

| | Cells (/ml) | Cells (/ml) | Deviation | Error | Average | |
|---|---|---|---|---|---|---|
| C+Au | 1.14E+06 | 1.02E+06 | 84852.81 | 60009.06 | 1.08E+06 | |
| C | 6.75E+05 | 1.13E+06 | 209418.8 | 104709.4 | 9.79E+05 | |
| C | 1.11E+06 | 1.01E+06 | | | | |
| Si | 6.90E+05 | 4.35E+05 | 108512.7 | 54256.34 | 5.63E+05 | |
| Si | 6.00E+05 | 5.25E+05 | | | | |
| P | 6.60E+05 | 6.00E+05 | 51234.75 | 25617.38 | 6.68E+05 | |
| P | 6.90E+05 | 7.20E+05 | | | | |
| | | | | | | |
| | | | | | | |
| | | | | | | |
| | | | | | | |
| | | | | | Seeding cell concentration (Cell/ml) | 2.60E+05 |
| | | | | | Cells per plate | 7.80E+05 |

**Table 5: Cell Adhesion Trial 2 (Method 2)**

| | Cells (/ml) | Cells (/ml) | Deviation | Error | Average | |
|---|---|---|---|---|---|---|
| C + Au | 1.06E+06 | 9.00E+05 | 100000 | 50000 | 1.03E+06 | |
| C + Au | 1.02E+06 | 1.14E+06 | | | | |
| C | 1.18E+06 | 1.32E+06 | 98994.95 | 70010.57 | 1.25E+06 | |
| P | 8.20E+05 | 7.40E+05 | 88459.03 | 44229.52 | 7.33E+05 | |
| P | 7.60E+05 | 6.10E+05 | | | | |
| Si | 5.50E+05 | 4.60E+05 | 81394.1 | 40697.05 | 4.43E+05 | |
| Si | 3.70E+05 | 3.90E+05 | | | | |
| | | | | | | |
| | | | | | Seeding cell concentration(cell/ml) | 3.63E+05 |
| | | | | | Cells per plate | 1.09E+06 |

**Table 6: Adhesion on Gold NPs of different concentrations (Method 2)**

| | Cells (/ml) | Cells (/ml) | Deviation | Error | Average | |
|---|---|---|---|---|---|---|
| C + Au (0.5) | 3.70E+05 | 3.90E+05 | 120568.1 | 49211.47 | 4.38E+05 | |
| C + Au (0.5) | 4.20E+05 | 2.90E+05 | | | | |
| C + Au (0.5) | 6.20E+05 | 5.40E+05 | | | | |
| C + Au (1.0) | 6.30E+05 | 6.50E+05 | 84083.29 | 34319.71 | 5.55E+05 | |
| C + Au (1.0) | 4.60E+05 | 4.80E+05 | | | | |
| C + Au (1.0) | 5.00E+05 | 6.10E+05 | | | | |
| C + Au (3.0) | 7.50E+05 | 8.10E+05 | 84241.72 | 34384.37 | 7.92E+05 | |
| C + Au (3.0) | 9.40E+05 | 8.00E+05 | | | | |
| C + Au (3.0) | 6.90E+05 | 7.60E+05 | | | Seeding cell concentration (Cell/ml) | 2.20E+05 |
| | | | | | Cells per plate | 6.60E+05 |

**Table 7: Cell Adhesion (Method 1)**

| | Cells (/ml) |
|---|---|
| C + Au (NGF) | 6.40E+05 |
| C + Au (NGF + PL) | 5.00E+05 |
| C + Au (PL) | 4.00E+05 |
| C + FeO (NGF) | 5.20E+05 |
| C + FeO (NGF +PL) | 5.80E+05 |
| C + FeO (PL) | 3.50E+05 |
| C + FeO (Bare) | 5.70E+05 |
| C (NGF) | 4.60E+05 |
| C (NGF +PL) | 4.10E+05 |
| C (PL) | 2.50E+05 |
| C (Bare) | 1.15E+06 |

**Table 8: Surface Energy (Water)**

| Water | | | | |
|---|---|---|---|---|
| | 1ml Au | Carbon | 0.5ml Au | 3ml Au |
| **Contact Angle** | 24.7 | 24.4 | 36 | 24.3 |
| | 26 | 36.8 | 32.7 | 29.5 |
| | 29.8 | 34.4 | 51.6 | 28.8 |
| | 32.2 | 35.7 | 41.2 | 28.2 |
| | 32 | 34.5 | 36.8 | 28 |
| | 25.9 | 85.2 | 40 | 28.5 |
| | 28.9 | 76.5 | 32.4 | 28.5 |
| | 40.2 | 79.4 | 34.3 | 28.7 |
| | 51.4 | 73.4 | 42.2 | 28.5 |
| | 47.4 | 82.4 | 46.6 | 28.2 |
| | 29.3 | 76 | 28.8 | 23.7 |
| | 30 | 76.9 | 28 | 22.1 |
| | 27.4 | 75.4 | 27.2 | 26.6 |
| | 25.5 | 79.6 | 26.5 | 30.2 |
| | 28 | 81.1 | 35.8 | 40.1 |
| **Average** | 31.91333 | 63.44667 | 36.00667 | 28.26 |
| **Standard Dev.** | 8.072605 | 22.51447 | 7.310215 | 3.994604 |
| **Uncertainty** | 2.084338 | 5.81321 | 1.887489 | 1.031402 |
| | | | | |
| **Surface Energy** | 137.4126 | 137.5692 | 130.2492 | 137.621 |
| | 136.7132 | 129.6527 | 132.5888 | 134.6656 |
| | 134.4791 | 131.4082 | 116.7226 | 135.0941 |
| | 132.9259 | 130.47 | 126.1739 | 135.4538 |
| | 133.0595 | 131.3371 | 129.6527 | 135.5722 |
| | 136.7682 | 78.0248 | 127.1552 | 135.2748 |
| | 135.0334 | 88.80807 | 132.7916 | 135.2748 |
| | 126.9933 | 85.2445 | 131.4791 | 135.1545 |
| | 116.9193 | 92.56956 | 125.3379 | 135.2748 |
| | 120.7351 | 81.52246 | 121.4703 | 135.4538 |
| | 134.789 | 89.41838 | 135.0941 | 137.9277 |
| | 134.3538 | 88.31889 | 135.5722 | 138.7101 |
| | 135.9227 | 90.14899 | 136.038 | 136.3791 |
| | 136.9861 | 84.99738 | 136.4353 | 134.2278 |
| | 135.5722 | 83.13915 | 130.3966 | 127.0743 |
| **Average** | 132.5776 | 101.5086 | 129.8105 | 135.2772 |
| **Standard Dev.** | 6.166097 | 22.7264 | 5.637022 | 2.59777 |
| **Uncertainty** | 1.592079 | 5.867931 | 1.455473 | 0.670741 |

**Table 9: Surface Energy (Formamide)**

| Formamide | | | | |
|---|---|---|---|---|
| | 1ml Au | Carbon | 0.5ml Au | 3ml Au |
| **Contact Angle** | 65.8 | 67.6 | 54.8 | 13.2 |
| | 65.8 | 41.1 | 50.3 | 12.8 |
| | 65.4 | 41.8 | 45.4 | 6.2 |
| | 61.2 | 38 | 61.9 | 49.7 |
| | 60.9 | 47.6 | 28.7 | 38.9 |
| | 54.8 | 55.2 | 21 | 54.3 |
| | 52.2 | 50.3 | 20.6 | 57 |
| | 45.1 | 52.4 | 34.1 | 50.3 |
| | 27.7 | 45.5 | 22.8 | 55 |
| | 27.3 | 49.8 | 21.2 | 55.1 |
| | 50.3 | 59.7 | 39.4 | 58.2 |
| | 45.1 | 43.7 | 42.8 | 51.2 |
| | 46.3 | 55.4 | 44.9 | 48.4 |
| | 49.2 | 54.6 | 43.2 | 51.4 |
| | 58.2 | 59.2 | 25.1 | 49.3 |
| **Average** | 51.68666667 | 50.79333 | 37.08 | 43.4 |
| **Standard Dev.** | 12.27121293 | 8.0996 | 13.41535 | 17.56356 |
| **Uncertainty** | 3.168413553 | 2.091308 | 3.463829 | 4.534891 |
| | | | | |
| **Surface Energy** | 81.77553596 | 80.10208 | 91.43307 | 114.4676 |
| | 81.77553596 | 101.7067 | 95.04853 | 114.5587 |
| | 82.14428595 | 101.2376 | 98.72488 | 115.6608 |
| | 85.9417131 | 103.7046 | 85.31869 | 95.51381 |
| | 86.20745206 | 97.10954 | 108.8745 | 103.1381 |
| | 91.43307434 | 91.10139 | 112.1477 | 91.84539 |
| | 93.54860911 | 95.04853 | 112.2915 | 89.58906 |
| | 98.9405511 | 93.38842 | 106.0275 | 95.04853 |
| | 109.3528303 | 98.65274 | 111.4681 | 91.26743 |
| | 109.5397995 | 95.43655 | 112.0748 | 91.18446 |
| | 95.04853342 | 87.2626 | 102.8185 | 88.56344 |
| | 98.9405511 | 99.93209 | 100.5563 | 94.34302 |
| | 98.07117984 | 90.93494 | 99.08371 | 96.50772 |
| | 95.89839503 | 91.59831 | 100.2802 | 94.18502 |
| | 88.56343614 | 87.69849 | 110.523 | 95.82171 |
| **Average** | 93.14543219 | 94.32764 | 103.1114 | 98.11298 |
| **Standard Dev.** | 9.014980677 | 6.415427 | 8.370097 | 9.345449 |
| **Uncertainty** | 2.327658002 | 1.656456 | 2.16115 | 2.412985 |

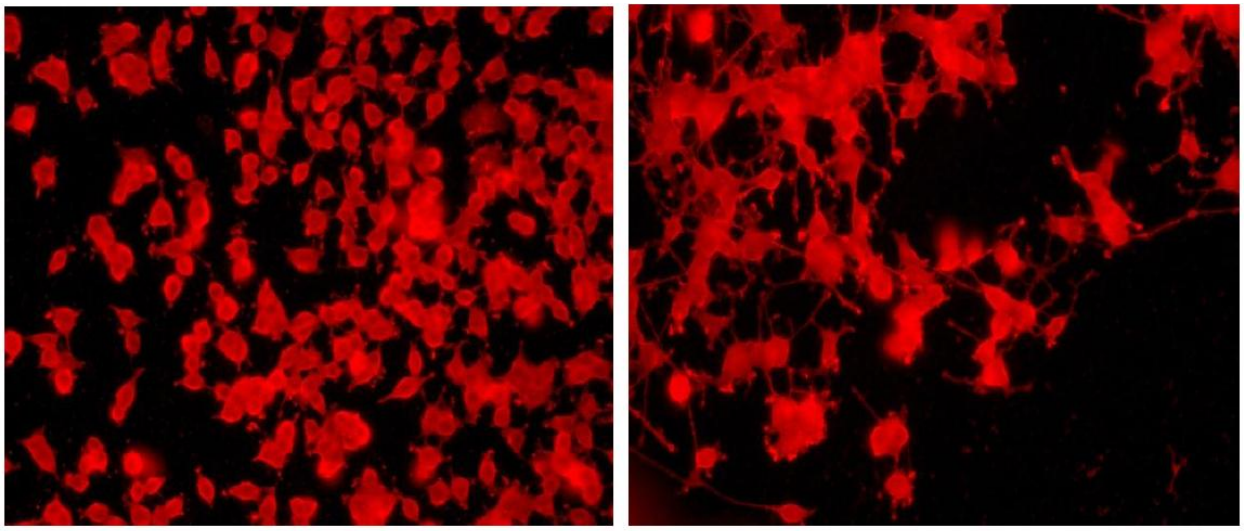

0.5ml Au 0.5ml Au+ NGF

**Figure 35: The effect of NGF on the 0.5ml Au samples**

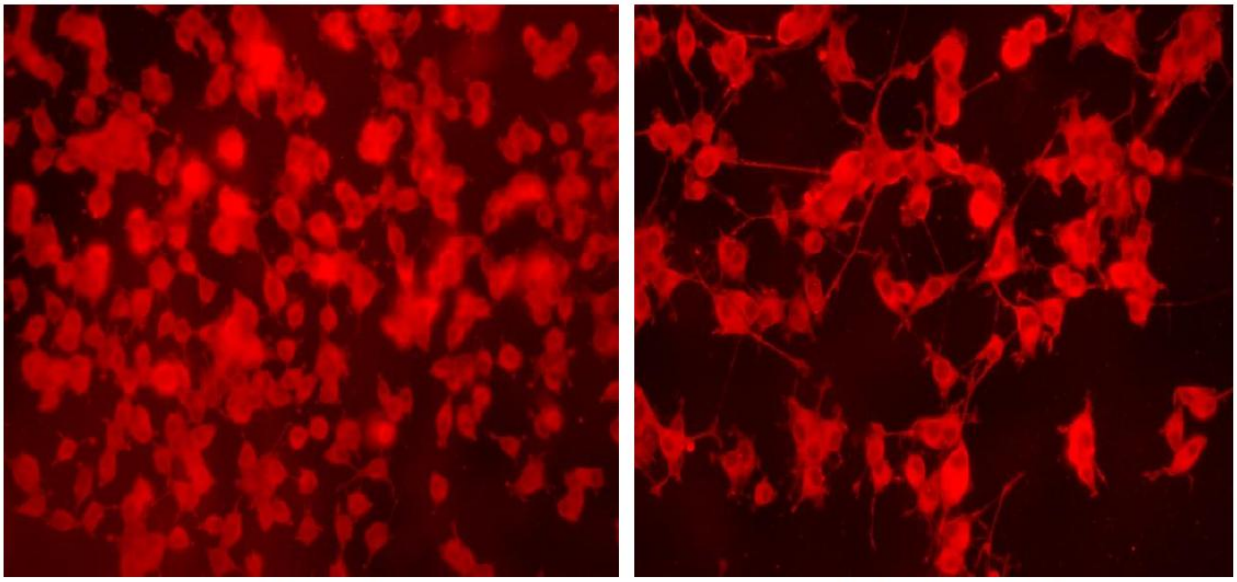

1.0ml Au 1.0ml Au+ NGF

**Figure 36: The effect of NGF on the 1ml Au samples**

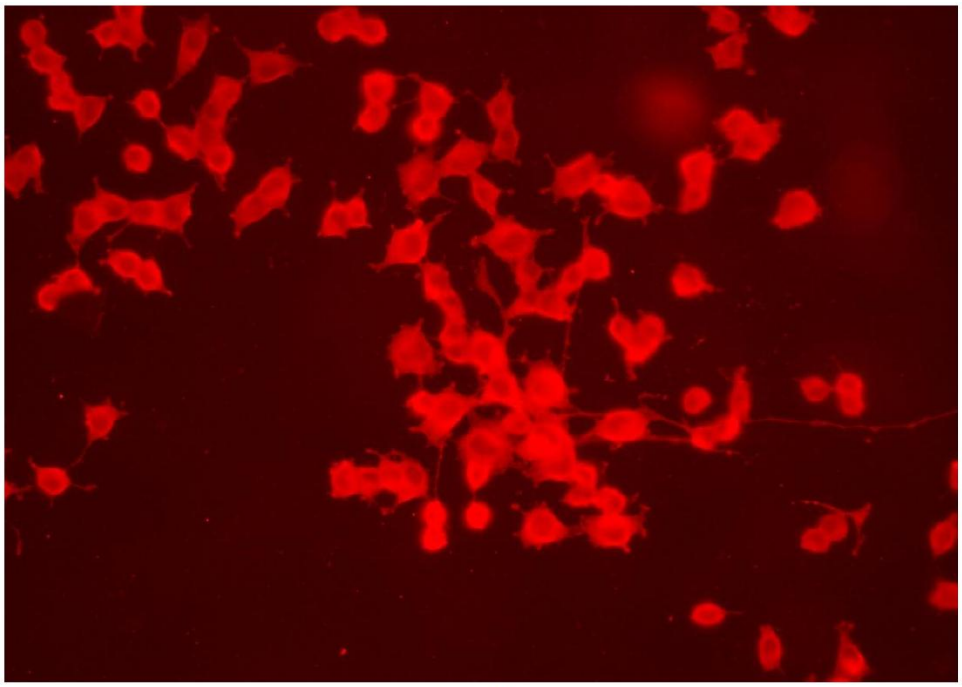

3.0ml Au

**Figure 37: Morphology of cells on the 3.0ml Au samples**

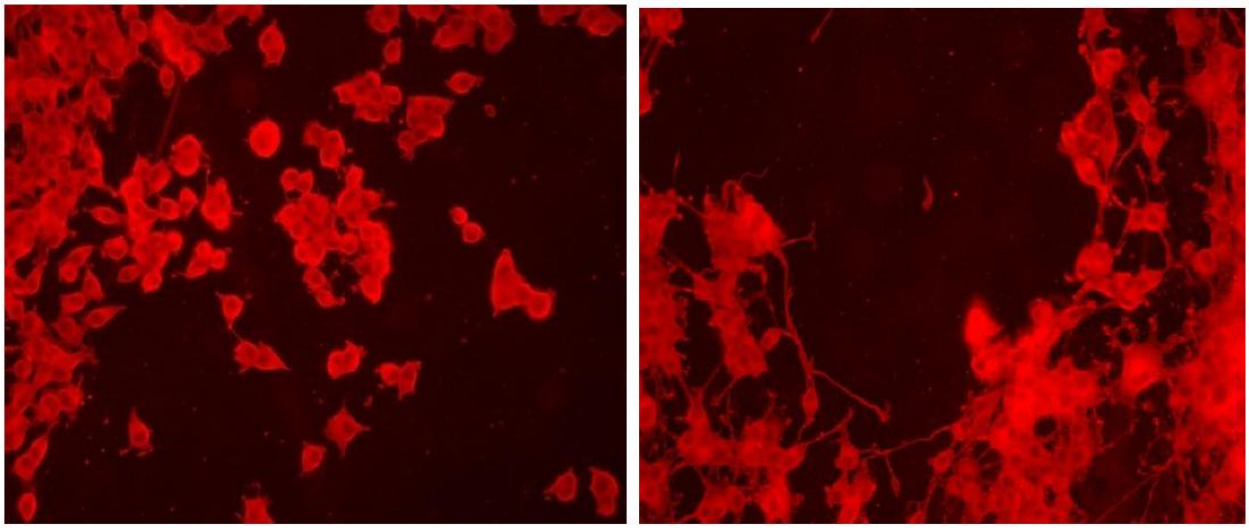

Glass+PL Glass+PL+NGF

**Figure 38: Effects of NGF on Glass+PL samples**